

新 制
理
975
京大附図

---

学位申請論文

---

---

小笠原 一禎

---

Thesis

Metallic Conduction of BO-Complex Conductive  
Langmuir-Blodgett Films,  
where BO is bisethylenedioxytetrathiafulvalene

Kazuyoshi Ogasawara

Department of Physics  
Faculty of Science  
Kyoto University

May 31, 1996

# Contents

<b>Abstract</b>	<b>3</b>
<b>1 Introduction</b>	<b>6</b>
1.1 Conductive Langmuir-Blodgett films	6
1.2 BO-C <sub>10</sub> TCNQ LB films	7
1.3 Molecular design based on the Hückel MO method	9
<b>2 Experimental</b>	<b>13</b>
2.1 Langmuir-Blodgett technique	13
2.2 Preparation of BO-C <sub>10</sub> TCNQ LB films	14
2.3 Electrical conductivity	15
2.4 X-ray diffraction	16
2.5 Electron spin resonance	16
2.6 Atomic force microscopy	17
2.7 Development of the BO-(MeO) <sub>2</sub> TCNQ LB film	17
<b>3 Experimental Results and Discussion</b>	<b>18</b>
3.1 Electrical conductivity	18
3.2 X-ray diffraction	18
3.3 Electron spin resonance	20
3.4 Atomic force microscopy	23
<b>4 Model Description</b>	<b>24</b>
4.1 MSI percolation model	24
4.2 Modified 2D MSI percolation model	26
4.3 Effect of domain shape on the dimensionality	30

4.4	Effective Medium Theory	31
4.5	Effective Medium Treatment of MSI percolation model	35
4.6	Phase diagram of the MSI percolation model	38
<b>5</b>	<b>Characterization of BO-(MeO)<sub>2</sub>TCNQ LB Film</b>	<b>40</b>
5.1	Electrical conductivity	40
5.2	X-ray diffraction	40
5.3	Electron spin resonance	41
5.4	Analysis based on the MSI percolation model	43
<b>6</b>	<b>Conclusion</b>	<b>44</b>
	<b>Acknowledgements</b>	<b>47</b>
	<b>References</b>	<b>48</b>

## Abstract

In recent years, Langmuir-Blodgett (LB) films of charge-transfer (CT) complexes have attracted increasing attention, because the LB technique is a useful method to construct well-organized organic multilayer films by manipulating monomolecular layers on the gas-liquid interface. However, those LB films usually possess disorders, and evaluation of disorder and its relation to electronic properties are important issue in this research field.

In this work, the structure and electronic properties of the conductive LB film consisting of bisethylenedioxytetrathiafulvalene- decyltetracyanoquinodimethane (BO-C<sub>10</sub>TCNQ) and icosanoic acid (IA) have been studied through the measurements of electrical conductivity, X-ray diffraction, electron spin resonance and atomic force microscopy for samples with different mixing ratio of the charge-transfer (CT) complex to IA molecules. We describe the preparation condition of highly conductive samples in details so as to include know-hows, since it had been essential for the present study and for future developments of this field.

The BO-C<sub>10</sub>TCNQ LB film exhibits metallic conduction without any secondary treatments. Although the conduction is brought about by the CT complex molecules, the insulating IA molecules are added as supporting material, which is necessary to apply the LB method. For one to one mixing ratio of C<sub>10</sub>TCNQ to IA, the maximum conductivity is 13.1 S/cm at room temperature and the conductivity increases by cooling down to 230 K, implying the presence of the macroscopic metallic conduction. With increase of the amount IA molecules, the room-temperature conductivity decreases and the metallic property is suppressed.

The X-ray diffraction measurements indicate coexistence of several domains with different interplanar spacings. The coherence length of the stacking structure estimated from the peak width is in the order of the film thickness, implying that the film is compartmentalized

in the film plane. In addition to the normal CT complex region and the IA region, a disordered CT complex region with an enlarged interplanar spacing is present in the BO-C<sub>10</sub>TCNQ LB films, presumably due to the involvement of water molecules.

The ESR measurements have shown that a Pauli-like paramagnetic susceptibility, which is insensitive to temperature variation, exists down to at least 50 K and the line width decreases with decreasing temperature. Taking into account the relatively large  $g$ -value, indicating rather large spin-orbit interaction, the behavior is ascribable to the Elliott mechanism, which is typical for conduction electrons. The semiconducting behavior in the macroscopic electrical conductivity below 230 K is probably due to the disordered CT complex region. From the anisotropy of ESR with respect to the film plane, it is concluded that CT complex molecules are well aligned so that the long axis of BO is directed perpendicular to the film plane.

The AFM imaging of the BO-C<sub>10</sub>TCNQ LB films shows that needle-like domains increase with increase of the CT complex molecules, indicating that the CT complex region forms needle-like domains.

In order to understand the temperature dependence of the electrical conductivity, we adopt a two-dimensional percolation model consisting of three kinds of sites, such as metallic, semiconducting and insulating sites (MSI percolation model). The percolation threshold of the BO-C<sub>10</sub>TCNQ LB film is lower than that of two-dimensional close-packed lattice, indicating that the effective dimension is more than two in the present system. This is due to the unevenness of the layer (percolation effect in the stacking direction) and the effect of the domain shape. The parameters are re-scaled according to the effective dimension so as to apply the simulation in two-dimension and the characteristic behavior of the conductance is reproduced well by this model. The effect of domain shape on the percolation threshold was also studied using a simulation with needle-like domains.

In addition to the simulation, the approximate expression of the conductivity for the MSI percolation model was calculated using the effective medium theory. The characteristic behavior of the electrical conductivity is interpreted in terms of effective dimension of the CT complex region. Based on the MSI percolation model, we derived a phase diagram describing the conducting properties and discussed the methods to realize better conductors.

In order to improve the metallic properties of the BO-C<sub>10</sub>TCNQ LB film, we searched a more appropriate constituent molecules taking into account the charge distribution within the molecules and self-assembling ability of BO molecules. As a result, a stable, highly conductive Langmuir-Blodgett film was developed using a CT complex of BO and dimethoxytetracyanoquinodimethane ((MeO)<sub>2</sub>TCNQ). A clear negative temperature-derivative of the conductivity was observed down to 180 K, indicating the establishment of the macroscopic metallic conduction. The X-ray diffraction measurements indicate the coexistence of three kinds of structures. The anisotropy of the ESR spectra shows that the CT complex molecules are highly oriented in the stacking direction. The Pauli-like paramagnetic spin susceptibility and the Elliott-like behavior of the line width indicate that the metallic phase is retained down to 50 K even if they are compartmentalized by the IA molecules and disordered regions. The temperature dependence of the electrical conductivity is also understood well by the MSI percolation model.

# 1 Introduction

## 1.1 Conductive Langmuir-Blodgett films

Organic molecular films with controlled layered structure have attracted much attention as functional materials not only due to their exotic nature as ultrathin substances but also due to designability in molecular combinations and stacking. The conductive Langmuir-Blodgett (LB) film [1,2] is one of such materials. It is regarded as a stack of two-dimensional conductive sheets. As the film-forming materials, charge-transfer (CT) complexes are of particular interest, because they show various physical properties, *e. g.*, metallic electrical conduction, superconducting phenomenon, or low-dimensional antiferromagnetism, depending on its constituents and crystalline forms [3,4]. Following the initial report of Barraud *et al.* [5], a great number of conductive LB films have been developed based on many kinds of CT complexes, however, they usually require secondary treatments such as iodine doping, which increase disorders within the film. Although disorders sometimes show unique phenomenon such as atomic size effect in the X-ray diffraction [6-9], it suppresses the metallic property of conductive LB films.

The Langmuir-Blodgett film based on N-docosylpyridinium-bistetracyanoquinodimethane [Fig. 1, hereafter referred to as  $C_{22}Py(TCNQ)_2$ ] is the first example of conductive LB films without doping [10-12]. It showed a room-temperature conductivity of order of  $10^{-2}$  S/cm. In order to clarify the conduction mechanism, various studies were carried out such as infrared (IR) spectra and electron spin resonance (ESR). The temperature dependence of the spin susceptibility was explained by the random-exchange Heisenberg antiferromagnetic chain (REHAC) model, and the presence of 1D columnar structure of TCNQ was confirmed. However, the temperature dependence of the electrical conductivity is semiconducting rather than metallic as shown in Fig. 2.

The first macroscopically metallic LB film was realized using the charge-transfer (CT)



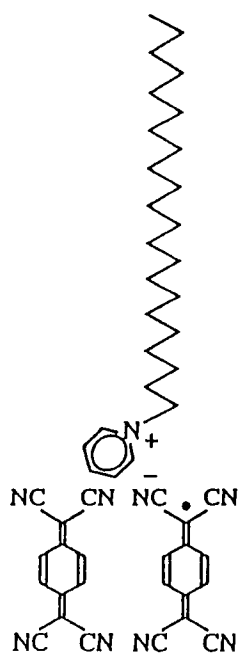


Fig. 1. Chemical structures of  $C_{22}Py(TCNQ)_2$ .

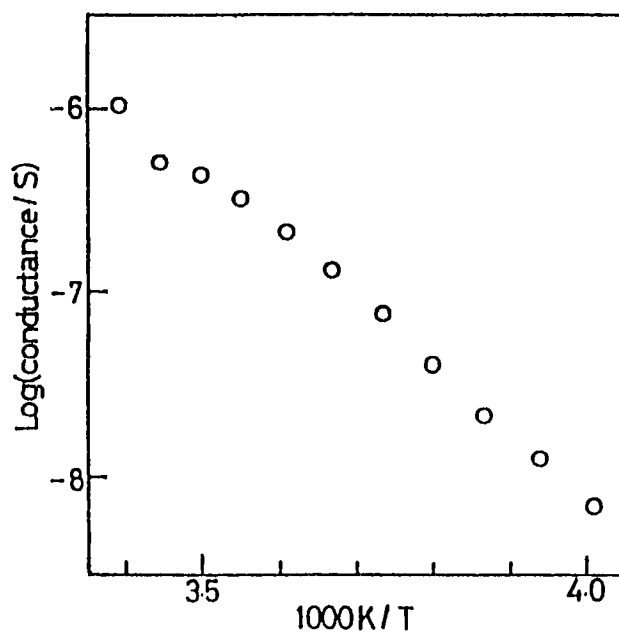


Fig. 2. Temperature dependence of electrical conductivity of  $C_{22}Py(TCNQ)_2$  LB film.

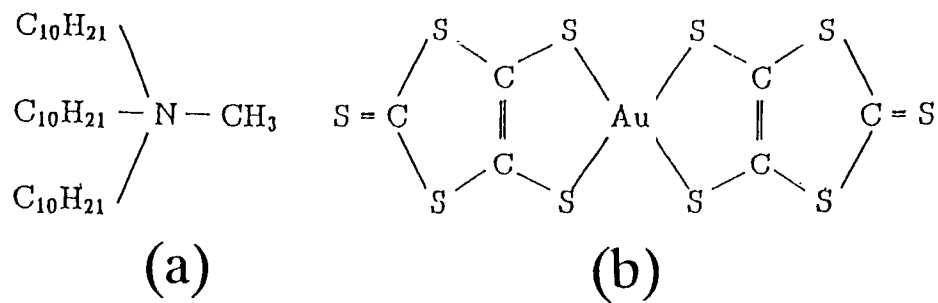


Fig. 3. Chemical structures of (a) 3C10 and (b) Au(dmit)<sub>2</sub>.

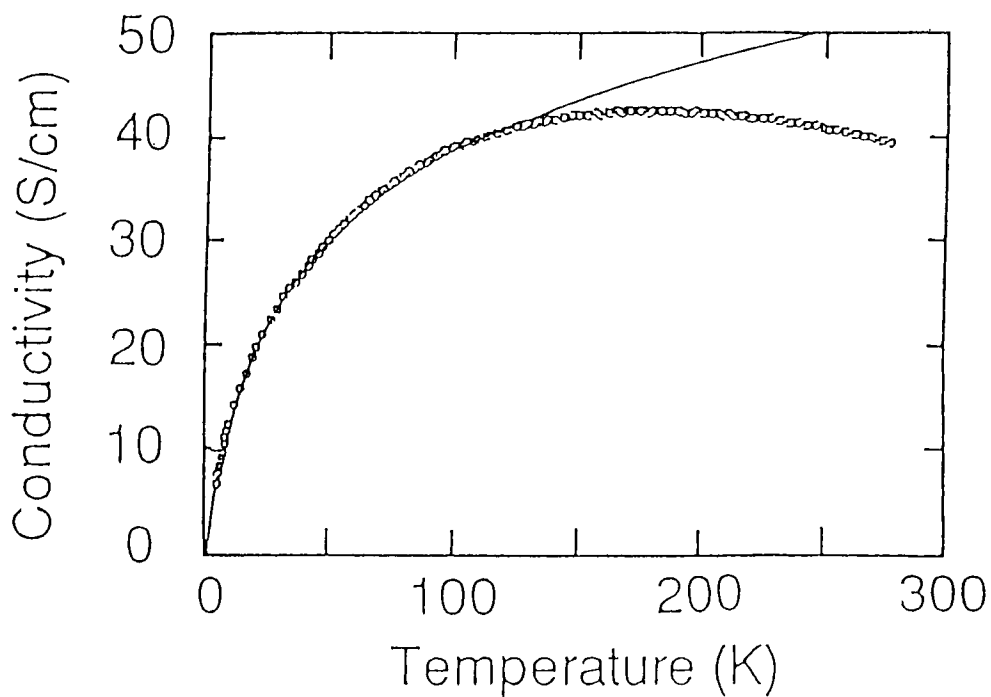


Fig. 4. Temperature dependence of electrical conductivity of 3C10-Au(dmit)<sub>2</sub> LB film.

complex of tridecylmethylammonium and bis(4, 5-dimercapto-1, 3-dithiole-2-thione)-gold [Fig. 3, hereafter referred to as 3C10 and Au(dmit)<sub>2</sub>, respectively ] [13,14]. The temperature dependence of the electrical conductivity is shown in Fig. 4. In order to characterize the metallic conduction, the structure and electronic properties have been studied extensively. However, for the realization of the metallic phase, an electrochemical oxidation is required and the film is not stable at ambient atmosphere. Thus the next important step in the development of conductive LB film had been to obtain a metallic LB film without any secondary treatments.

## 1.2 BO-C<sub>10</sub>TCNQ LB films

A macroscopic metallic LB film without any secondary treatments was realized using the CT complex of bisethylenedioxytetrathiafulvalene (BO) and decyltetracyanoquinodimethane (C<sub>10</sub>TCNQ) [Fig. 5] [15]. A gradual metal-nonmetal transition is observed around 250 K and the temperature dependence of the electrical conductivity turns to be semiconducting below that temperature. Due to the presence of icosanoic acid (IA) molecules [Fig. 5], which is necessary as supporting material to apply the LB method, the film is not a homogeneous conductor. From physical point of view, the film can be regarded as an interesting system to study the electrical conduction in inhomogeneous conductors, because the mixing ratio of CT complex to IA can be altered. In order to reveal the metallic behavior, the electronic properties have been studied in various ways. The thermoelectric power [16] and Hall resistance [17] indicate that the major charge carriers in the film are holes. From the IR spectra [16], the charges on the BO and C<sub>10</sub>TCNQ moieties are estimated as +0.4 and -1.0, respectively.

The temperature dependence of the electrical conductivity has been explained by a boundary model as described below. Dividing the two-dimensional film into  $n$  strips parallel to the applied voltage, the resistance of the  $i$ -th strip ( $R_i$ ) is given using the conductivities

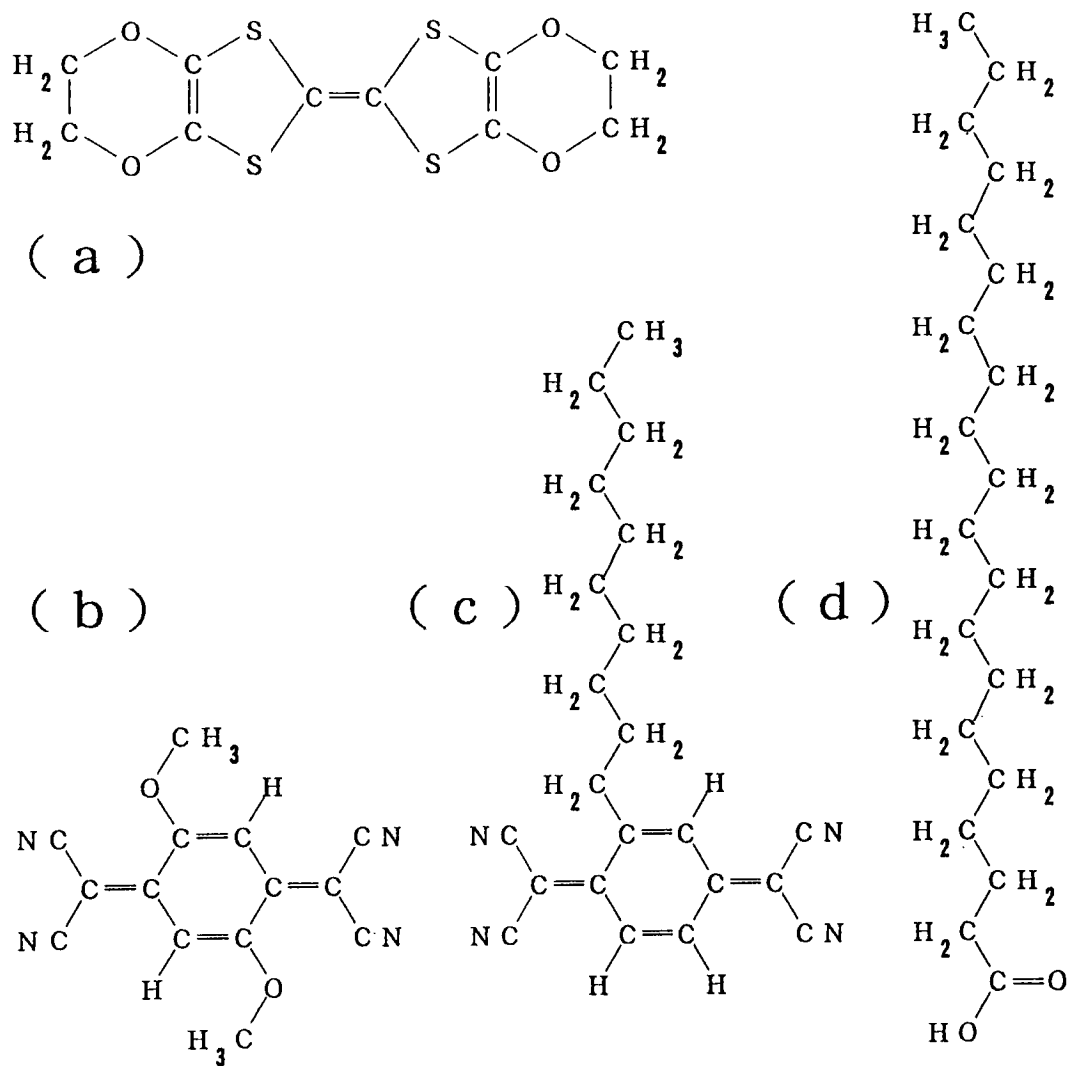


Fig. 5. Chemical structures of (a) BO, (b) (MeO)<sub>2</sub>TCNQ, (c) C<sub>10</sub>TCNQ and (d) IA.

of the domain ( $\sigma_m$ ) and the domain boundary ( $\sigma_b$ ) as

$$R_i = \frac{n(1 - r_{bi})L}{A} \frac{1}{\sigma_m} + \frac{nr_{bi}L}{A} \frac{1}{\sigma_b}, \quad (1)$$

where  $r_{bi}$ ,  $L$ ,  $A$  are the fraction of domain boundaries in the  $i$ -th strip, the total length and the cross-sectional area of the sample, respectively. The total resistance  $R$  is written as,

$$\frac{1}{R} = \sum_i \frac{1}{R_i} = \frac{A}{nL} \sum_i \left\{ \frac{\sigma_m \sigma_b}{(1 - r_{bi})\sigma_b + r_{bi}\sigma_m} \right\} \simeq \frac{A\sigma_b}{nL} \sum_i \frac{1}{r_{bi}}, \quad (2)$$

where  $r_{bi}\sigma_m \gg (1 - r_{bi})\sigma_b$  is assumed since the conductivity in the domain is much larger than that in the domain boundary. Thus, the temperature dependence is completely dominated by the domain boundary, which has been regarded as a semiconductor described by the equation proposed by Epstein *et al.* [18,19],

$$\sigma = AT^{-\alpha} \exp\left(-\frac{E}{kT}\right), \quad (3)$$

where  $A$  and  $\alpha$  are constants,  $k$  the Boltzmann constant and  $E$  the band gap. In this model, the gradual metal-nonmetal transition was ascribed to the intrinsic nature of the domain boundary. The temperature dependence of the conductivity for the BO-C<sub>10</sub>TCNQ LB film can be phenomenologically fitted by this model [16]. Experimentally, the temperature dependence of the conductivity is strongly affected by the mixing ratio of the CT complex to IA, indicating the variation of fitting parameters such as  $A$ ,  $\alpha$  and  $E$  depending on the ratio. However, the physical interpretation of the variables is indistinct. Taking into account that the film is an inhomogeneous system, it is natural to consider the conduction is brought about by percolation path. In other words, the conductivity should be understood in relation with the mesoscopic structure of the film.

The major subject of this article is to present the investigation on the relationship between structure and electronic properties within the BO-C<sub>10</sub>TCNQ LB films through the measurements of the electrical conductivity, X-ray diffraction and ESR for films prepared

with different ratio of the CT complex to IA. The results of X-ray diffraction and ESR indicate the coexistence of metallic domains, semiconducting domains and insulating domains. In order to explain the temperature dependence of the conductivity, we propose a percolation system consisting of three kinds of sites, which we call metal-semiconductor-insulator (MSI) percolation model. An ideal LB film can be regarded as a typical two-dimensional system but the present film with domain structure cannot be ruled by the two-dimensionality. In order to characterize the conductivity, the effect of dimensionality is taken into account through the re-scaling of the parameters. Then, the experimental data are compared with a numerical calculation based on the modified two-dimensional MSI percolation model. As a result, the overall characteristics, including the gradual metal-nonmetal transition, are interpreted in terms of the effect of percolation path without assuming any intrinsic metal-nonmetal transition. The variation depending on the mixing ratio of the constituent molecules is well reproduced by the variation of only one parameter, which is directly related to the ratio. In addition to the numerical simulation, the conductivity of the LB film is calculated using the effective medium theory with some modification. In this model, the variation of the temperature dependence of the electrical conductivity is clearly understood as the dimensionality effect of the CT complex region.

### **1.3 Molecular design based on the Hückel MO method**

The characteristics of representative conductive LB films are summarized in Table 1,

In order to improve the metallic properties of conductive LB films, it is necessary to decrease disorder within the film. For this purpose, it is very important to develop a metallic LB film without doping nor supporting molecules, however, such film has not been obtained yet. For the realization of such a film, a proper design of the constituent molecules is indispensable. In order to seize the properties of molecules, the Hückel MO calculation is one of the useful methods, which is described below [4].

Table 1: Characteristics of representative conductive LB films.

CT Complex	Metallic	without doping	without supporting molecules
C <sub>22</sub> Py(TCNQ) <sub>2</sub>	No	Yes	Yes
3C10-Au(dmit) <sub>2</sub>	Yes	No	No
BO-C <sub>10</sub> TCNQ	Yes	Yes	No
?	Yes	Yes	Yes

The molecular orbitals are obtained by solving the one-electron Schrödinger equation,

$$h(\mathbf{r})\psi_m(\mathbf{r}) = \epsilon_m\psi_m(\mathbf{r}). \quad (4)$$

where  $\mathbf{r}_i$  is the position of the  $i$ -th electron,  $h(\mathbf{r})$  is a one-electron Hamiltonian, with eigenvalue  $\epsilon_m$  and eigenfunction  $\psi_m(\mathbf{r})$ . In the Hückel MO method, only  $\pi$ -electrons are taken into account. In order to solve Eq. (4), we approximate  $\psi_m$  by a linear combination of atomic orbitals  $\chi_p(\mathbf{r})$  for the atomic position specified by  $p$ ,

$$\psi_m(\mathbf{r}) = \sum_p C_{pm}\chi_p(\mathbf{r}). \quad (5)$$

The coefficients  $C_{pm}$  are determined from

$$\sum_p (h_{qp} - \epsilon_m S_{qp})C_{pm} = 0, \quad (6)$$

where,

$$\begin{cases} h_{qp} &= \int \chi_p^*(\mathbf{r})h(\mathbf{r})\chi_p(\mathbf{r})d\mathbf{r} \\ S_{qp} &= \int \chi_p^*(\mathbf{r})\chi_p(\mathbf{r})d\mathbf{r} \end{cases} \quad (7)$$

To make the problem simpler, we make the further approximation that

$$S_{qp} = \begin{cases} 1 & \text{for } q = p \\ 0 & \text{for } q \neq p \end{cases}, \quad (8)$$

and

$$h_{qp} = \begin{cases} \alpha_p & \text{for } q = p \\ \beta_{qp} & \text{when } q \text{ and } p \text{ are adjacent} \\ 0 & \text{otherwise} \end{cases}, \quad (9)$$

Table 2: List of parameters used in the Hückel calculation.  $n_\pi$  is the number of  $\pi$ -electrons within the atom.

	$n_\pi$	$\alpha_p$	$\beta_{pq}$	C	N2
C	1	0.00	C	1.00	0.89
N2	2	1.37	N2	0.89	0.98
O2	2	2.09	O2	0.66	0.89
S2	2	1.11	S2	0.69	0.73
C2	2	1.48	C2	0.62	0.80

where  $S_{qp}$ ,  $\alpha_p$  and  $\beta_{pq}$  are the overlap integral, the Coulomb integral and the resonance integral or transfer energy, respectively, and their values are estimated semi-empirically. For the actual calculation, we adopted the values presented by Van-Catledge [20], which is listed in Table. 2.

By solving Eq. (6) using above values, the MO's of BO and TCNQ were calculated and numbered in order of increasing energy. Taking into account the spin degeneracy, the HOMO is represented by the  $(N_\pi/2)$ -th MO, while the LUMO is represented by the  $(N_\pi/2 + 1)$ -th MO, where  $N_\pi$  is the number of  $\pi$ -electrons within the molecule. The calculated HOMO of BO and the LUMO of TCNQ are illustrated in Fig. 6, where the area of each shaded circle is proportional to the number density of the  $\pi$ -electrons. Apparently, the HOMO of BO is concentrated mainly in the central part of the molecule, while the LUMO of TCNQ is concentrated in the outer ends of the molecule. When charge transfer occurs between them, electrons are added to the latter while holes are created in the former. Considering the coupling between the charged orbitals and polarized water molecules, TCNQ tends to be hydrophilic. However, BO becomes rather hydrophobic due to the hydrophobic ethylene groups existing at the outer ends of the molecules. In addition, due to a strong self-assembling ability of BO [27], the charge transfer molecular pairs form an amphiphilic sheet with a pair of hydrophilic and hydrophobic surfaces. In other words, a pair of BO and



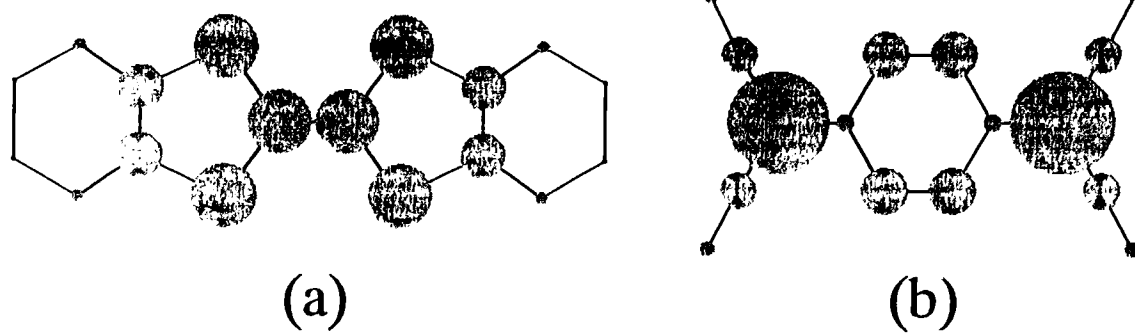


Fig. 6. (a) HOMO of BO and (b) LUMO of TCNQ. The area of each shaded circle is proportional to the number density of  $\pi$  electrons at each atomic site.

TCNQ molecules is expected to possess a potential to create an amphiphilic CT complex by itself. In this respect the addition of the long alkyl chain to TCNQ (like C<sub>10</sub>TCNQ) is not necessary and may in fact work as a hindrance to the formation of a regular arrangement of the CT complex molecules, resulting in increased disorder.

With this point of view, we have searched for a TCNQ derivative which forms a metallic CT complex with BO and possesses an amphiphilic nature to obtain an LB film. We found that the CT complex of BO and dimethoxytetracyanoquinodimethane ((MeO)<sub>2</sub>TCNQ) [Fig. 5] forms a stable, highly conductive LB film, with the addition of IA as a matrix. This is an original achievement but is described in a subsidiary way in this article. Although the new material requires the supporting molecules, metallic properties are considerably improved compared to the BO-C<sub>10</sub>TCNQ LB film.

## 2 Experimental

### 2.1 Langmuir-Blodgett technique

The Japanese "sumi nagashi" technique of forming monolayers at a water surface and depositing the film on a solid support was invented about 1000 years ago and is still in use. It is the first example of engineering at the molecular level: Chinese ink, a suspension of carbon particles in a protein solution, is spread on a water surface, and a protein monolayer is formed, which is picked up by paper, using the horizontal lifting technique. Agnes Pockels, 100 years ago, realized when pushing together a soap film at a water surface, that the film pressure increased strongly below a certain area [21-23], and Rayleigh concluded that this is due to the formation of a monomolecular layer and obtained a value for the size of a surfactant molecule [24], at a time when many scientists did not believe in the reality of atoms. Langmuir and Blodgett studied the detailed structure of fatty acid multilayers obtained by depositing monolayers on a glass slide on top of each other and investigated the detailed conditions for producing such films [25,26].

Monolayer-forming molecules typically possess both hydrophobic and hydrophilic groups and are called amphiphiles. If the balance between both groups is appropriate, the molecules remain at the air-water interface when their solutions in volatile solvent are spread onto the water surface. The monolayer on a water surface is a two-dimensional system, as shown schematically in Fig. 7. If the surface pressure  $\pi$  is small enough, monolayer is in so-called "two-dimensional gas" or "two-dimensional liquid" state. On reducing the area per molecule  $A$ ,  $\pi$  increases and the monolayer is transformed into the so-called "two-dimensional solid" state, in which the compressibility of the monolayer is relatively small. After evaporation of the solvent, the monolayer is compressed by the moving barrier. By setting an appropriate value of  $\pi$ , the monolayer is kept in the "solid" state.

In the vertical dipping method, a solid substrate is vertically dipped and raised across the

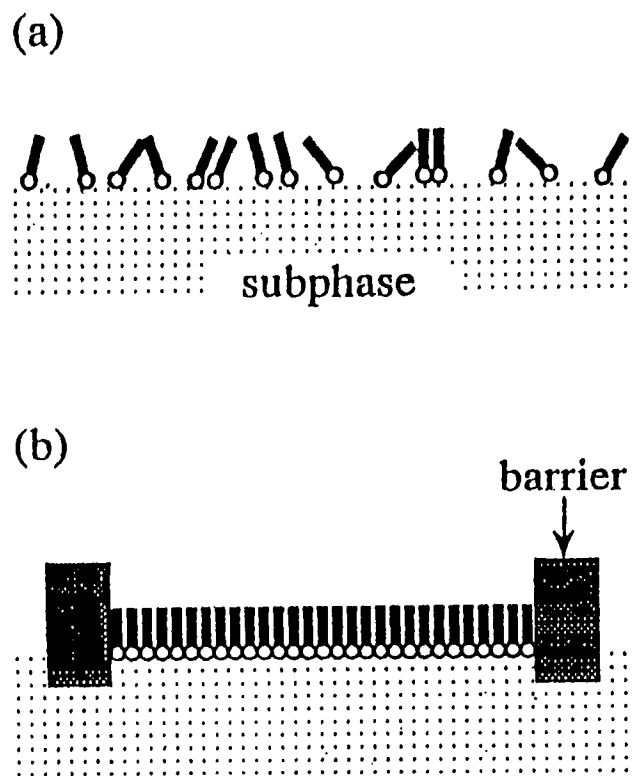


Fig. 7. Schematic illustrations of a monolayer on the air-water interface. (a) a "two-dimensional gas" state and (b) a "two-dimensional solid" state.

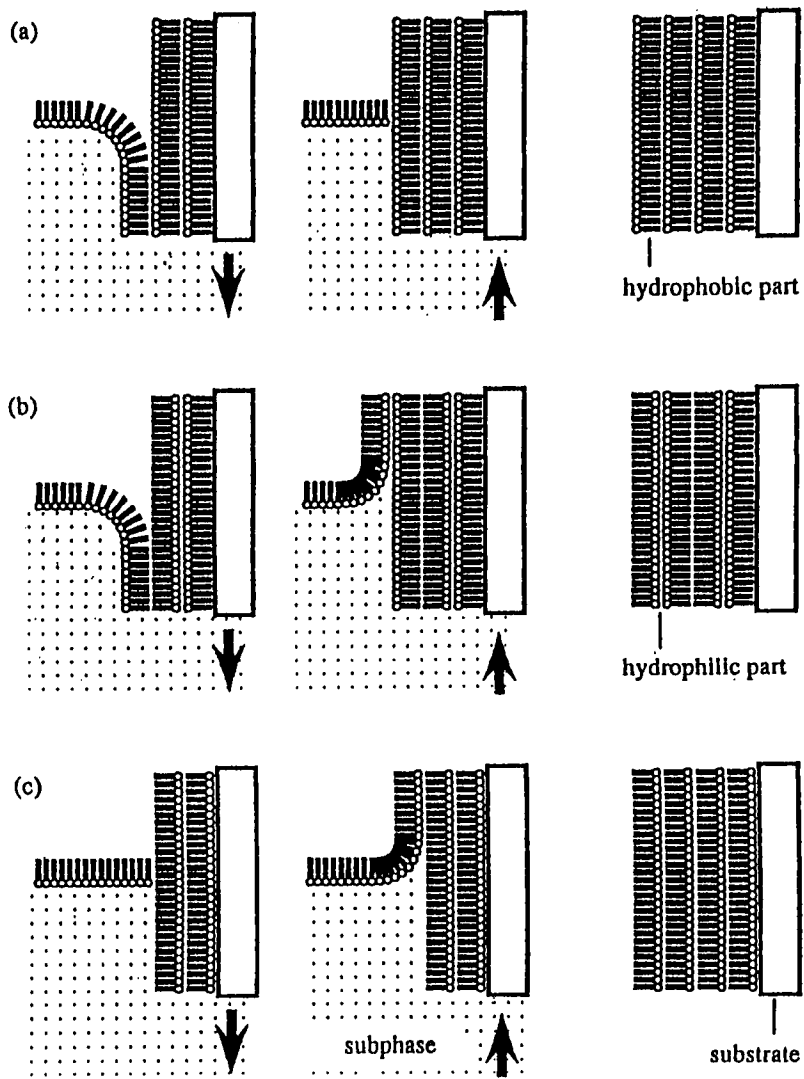


Fig. 8. Schematic illustrations of the vertical dipping method. There are three types of staking structures: (a) X-type, (b) Y-type and (c) Z-type.

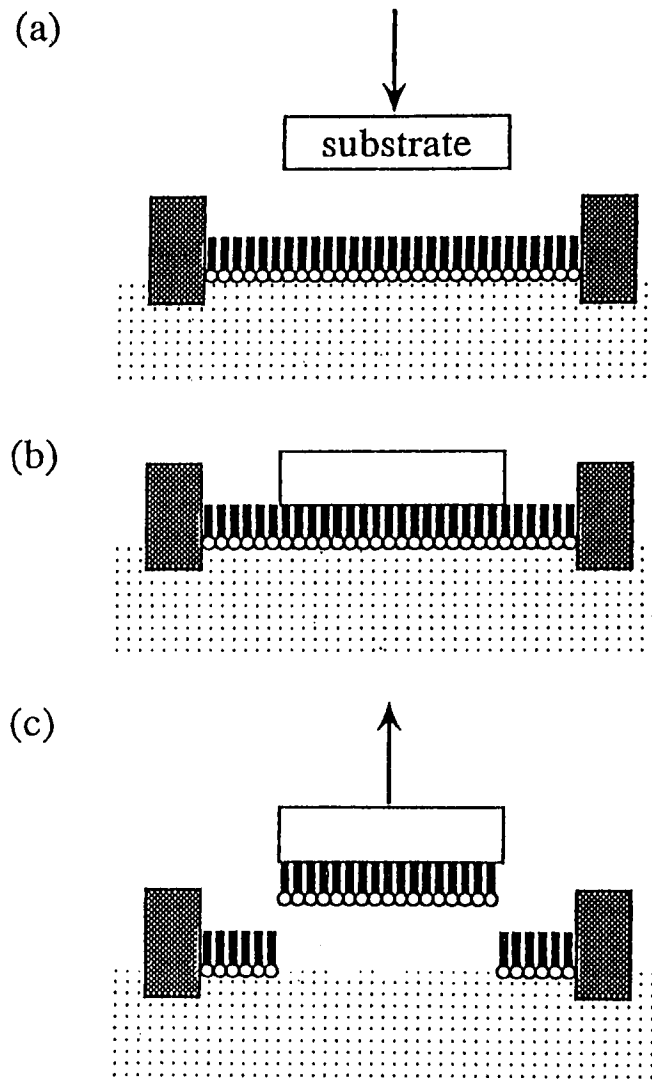


Fig. 9. Schematic illustration of the horizontal lifting method.

water surface [Fig. 8]. Depending on the monolayer-forming material and the deposition conditions, such as temperature and hydrophilicity of the substrate, the monolayer may be transferred during both the dipping and raising strokes (Y-type), only the dipping strokes (X-type), or only the raising strokes (Z-type). The decrease in the area of the monolayer divided by the area of the substrate surface is called the transfer ratio, which characterizes the deposition process and is unity or zero in the ideal deposition cases. This method was developed by Langmuir and Blodgett [25,26].

In the horizontal lifting method, on the contrary, the substrate is held horizontally and is lowered onto the monolayer from above [Fig. 9]. The resulting films have the X-type structure with a single-layer unit cell in the ideal deposition case. Although the vertical dipping method is more appropriate for the conventional film forming materials such as cadmium arachidate, the horizontal lifting method produces better quality films for the BO-C<sub>10</sub>TCNQ LB films [15].

## 2.2 Preparation of BO-C<sub>10</sub>TCNQ LB films

The BO-C<sub>10</sub>TCNQ LB films were prepared by the horizontal lifting method. The ultrapure water with resistivity of more than 18 MΩ cm was used as the subphase. Flat-surface glass plates with the planar dimension of 13 mm × 39 mm and the thickness of 1 mm were used as substrates. They were hydrophobized by soaking in the 1, 1, 1, 3, 3, 3-hexamethyldisilazane for 1 h. before deposition. The acetonitrile solution of 5 : 2 complex of BO and C<sub>10</sub>TCNQ ( $5 \times 10^{-4}$  mol/l in unit of C<sub>10</sub>TCNQ) and the benzene solution of IA ( $5 \times 10^{-4}$  mol/l) were mixed with volume ratio of 1 :  $X$  and spread on the water subphase kept at 290 K. Here,  $X$  was varied from 1 to 6.

Waiting a certain time ( $T_1$ ), the monolayer on the subphase was compressed with the barrier speed of 2.0 cm/min. until the surface pressure becomes 20 mN/m. Waiting another interval ( $T_2$ ) after the compression, the Langmuir film on the subphase was divided into

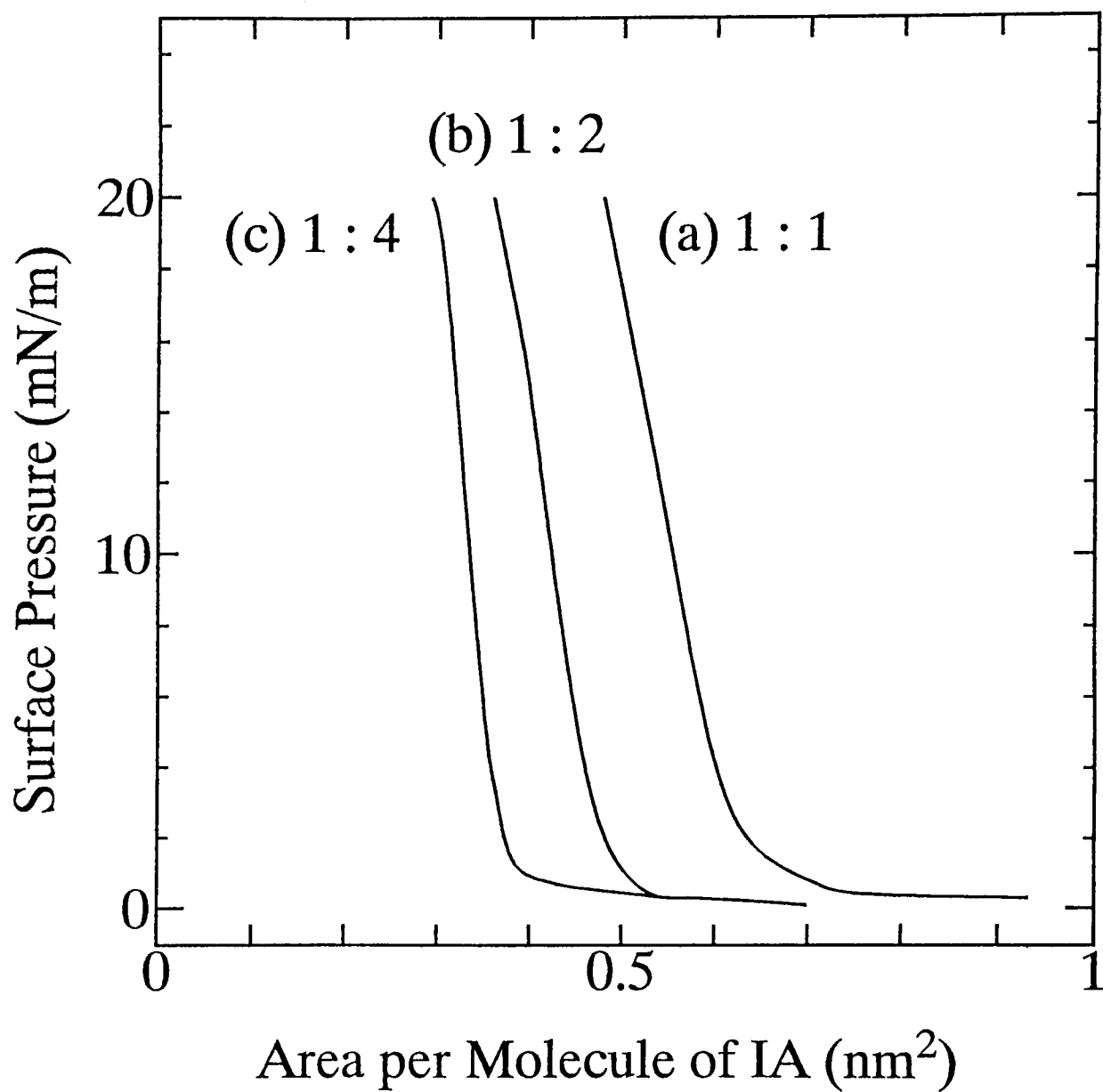


Fig. 10.  $\pi$ -A isotherms of the mixed monolayer of BO-C<sub>10</sub>TCNQ and IA on the water surface with (a) 1 : 1, (b) 1 : 2 and (c) 1 : 4 ratio.



24 sections using a teflon coated areal divider. The area of each section is  $15 \text{ mm} \times 41 \text{ mm}$ , a little larger than the area of the substrate. After waiting another interval ( $T_3$ ), the Langmuir film was deposited onto the substrate 20 times within a certain time ( $T_4$ ). We have experienced that the conductivity of the deposited LB film is strongly affected by the preparation condition, especially the waiting time such as  $T_i$  ( $i = 1, 2, 3, 4$ ). Initially, we supposed that the larger values of  $T_i$ 's are preferable to obtain a stabilized LB film. However, we found that the conductivity of the resultant LB film decreases when we increase the values of  $T_i$ 's exceeding certain values. This implies that the CT complex on the water surface is not stable enough. Then we searched proper values of  $T_i$ 's to get an LB film with the maximum conductivity: a typical successful time sequence is given by  $T_1 = 15 \text{ min.}$ ,  $T_2 = 5 \text{ min.}$ ,  $T_3 = 5 \text{ min.}$  and  $T_4 = 30 \text{ min.}$  The films studied in this work were prepared under these conditions. The pressure-area ( $\pi$ -A) isotherms for  $X = 1, 2, 4$  are shown in Fig. 10. An abrupt increase of the surface pressure was observed below a certain critical area. A slight increase of the slope for larger  $X$  indicates that the Langmuir film on the water surface becomes more stable when prepared with larger amount of IA.

### 2.3 Electrical conductivity

For the measurements of the electrical conductivity, gold electrodes with thickness of 100 nm were evaporated on the hydrophobized surface of the glass substrate, before the deposition of the LB film. The distance between the gold electrodes was 0.5 mm and the width of the sample was 39 mm. Copper thin wires were attached using silver paste onto electrodes as leads. The temperature dependences of the electrical conductivity were measured for the BO-C<sub>10</sub>TCNQ LB films prepared with 1 :  $X$  ( $X = 1, 2, 3, 4$  and 6) ratio of C<sub>10</sub>TCNQ to IA (hereafter denoted by 1 :  $X$  film) by a dc four-probe method. Since we are interested in the  $X$  dependence of the metal-nonmetal transition observed in the high temperature region, we measured the temperature dependence down to the liquid nitrogen

temperature.

## 2.4 X-ray diffraction

In order to evaluate the structural order in the direction normal to the film plane and the domain structure within the film, X-ray diffraction measurements were carried out for the BO-C<sub>10</sub>TCNQ LB films (1 : X film with X = 1, 2, 4) deposited on the hydrophobized glass substrate. The measurements were performed by an ordinary  $\theta$ - $2\theta$  scan method with a CuK $\alpha$  source operated at 40 KV and 200 mA. Due to the lack of heavy atoms and the thinness of the film, such a large current was required. For comparison, the X-ray diffraction measurements of BO-C<sub>10</sub>TCNQ complex powder sample and a homogeneous LB film consisting of IA were also carried out.

## 2.5 Electron spin resonance

The ESR measurements were carried out for BO-C<sub>10</sub>TCNQ LB films (1 : X film with X = 1, 2, 4) deposited on the hydrophobized glass substrate which was inactive to the ESR, by using a Bruker ESP-300E spectrometer at the X band (9.4 GHz). Samples were cooled down to liquid helium temperature using an Oxford ESR900 cryostat and temperature dependence of the spectra was obtained. In order to evaluate the orientation of the molecules, the anisotropy was also studied by comparing the spectra obtained under dc magnetic fields parallel and perpendicular to the film plane. The spectra were accumulated 5 times in the temperature range of 50 – 190 K and 10 times above that temperature, because of the low signal to noise ratio reflecting the thinness of the film. The microwave power of 100 mw was needed to get appreciable signal to noise ratio.

## 2.6 Atomic force microscopy

The atomic force microscopy (AFM) measurements were carried out for BO-C<sub>10</sub>TCNQ LB films (1 : X film with X = 1, 2, 4) deposited on the hydrophobized glass substrate, by using a Epson SPA-300 scanning probe microscope system. The AFM topographic images of the film surface are obtained in the areas of 5 × 5 (μm<sup>2</sup>) and 10 × 10 (μm<sup>2</sup>) by the repulsive force mode with the force of 8.7 × 10<sup>-11</sup> N.

## 2.7 Development of the BO-(MeO)<sub>2</sub>TCNQ LB film

Based on the molecular design described in the section 1.3, a 2 : 1 complex of BO and (MeO)<sub>2</sub>TCNQ was selected as the constituent molecules of the conductive LB film. We first attempted to prepare an LB film using an acetonitrile solution of the CT complex (5 × 10<sup>-4</sup> mol/l in units of (MeO)<sub>2</sub>TCNQ), but we found that the surface pressure of the Langmuir film spread over the water subphase is not sufficiently strong to apply the LB method. Then, a benzene solution of IA (5 × 10<sup>-4</sup> mol/l) was mixed with volume ratio of 1 : 1 and spread on the water subphase. The resultant pressure-area (π-A) isotherm is shown in Fig. 11, where the area is represented in units of area per molecule of IA. An abrupt increase of the surface pressure below 0.4 nm<sup>2</sup> indicates the formation of stable Langmuir film. Flat-surface glass plates were used as substrates and they were hydrophobized by soaking in the 1, 1, 1, 3, 3, 3-hexamethyldisilazane for 1 h. The mixed monolayer on the water surface was easily transferred onto the substrate by the horizontal lifting method. Films studied here were deposited twenty times under a surface pressure of 20 mN/m at a water temperature of 290 K.

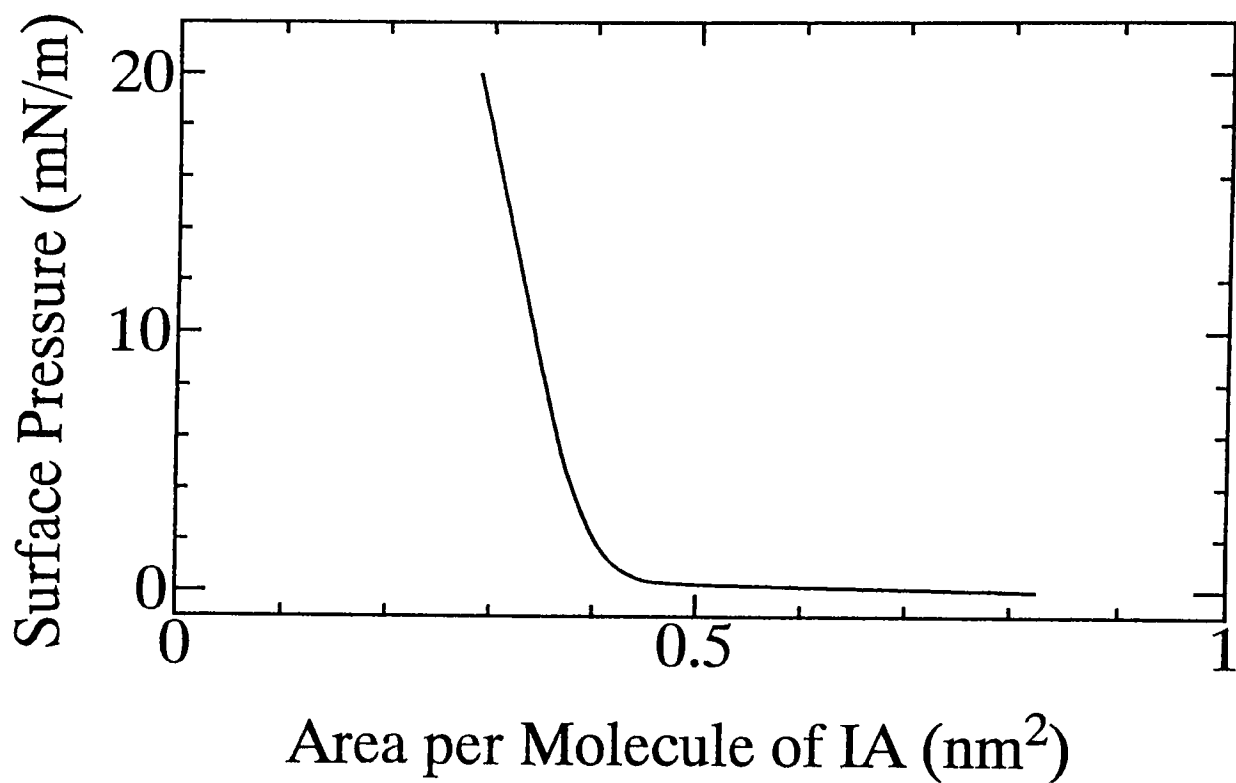


Fig. 11.  $\pi$ -A isotherm of the mixed monolayer of  $\text{BO}_2^-(\text{MeO})_2\text{TCNQ}$  and IA on the water surface at 290 K.

## 3 Experimental Results and Discussion

### 3.1 Electrical conductivity

The temperature dependences of the electrical conductivity for BO-C<sub>10</sub>TCNQ LB film (1 : X film with X = 1, 2, 4) are shown in Fig. 12, where the thickness of the monolayer is evaluated to be 2.5 nm [15]. For the 1 : 1 film, the room-temperature conductivity is 13.1 S/cm and shows a metallic temperature dependence (negative temperature-derivative) down to 230 K. The temperature dependence turns to be semiconducting (positive temperature-derivative) below that temperature. For the 1 : 2 film, the room-temperature conductivity is 7.0 S/cm and a metallic temperature dependence was also observed down to 260 K. For the 1 : 3 and 1 : 4 films, only semiconducting temperature dependence was observed. The variation of the room-temperature conductivity ( $\sigma_{RT}^{ob}$ ) and the temperature with the maximum conductivity ( $T_{max}^{ob}$ ) are listed in Table 3. Obviously, the metallic behavior is suppressed for larger value of X. When X is equal to 6, a conductive LB film could not be obtained.

Table 3: List of experimental parameters related to the electrical conductivity.

X	1	2	3	4
$\sigma_{RT}^{ob}$ (S/cm)	13.1	7.0	2.6	1.2
$T_{max}^{ob}$ (K)	230	260	—	—

### 3.2 X-ray diffraction

The observed diffraction profile for the BO-C<sub>10</sub>TCNQ complex powder sample is shown in Fig. 13(a). Two diffraction peak series representing different periodicity are observed. One (A series) corresponds to a periodic structure whose interplanar spacing is equal to 2.1 nm and the other (B series) corresponds to that equal to 2.4 nm. The diffraction profile

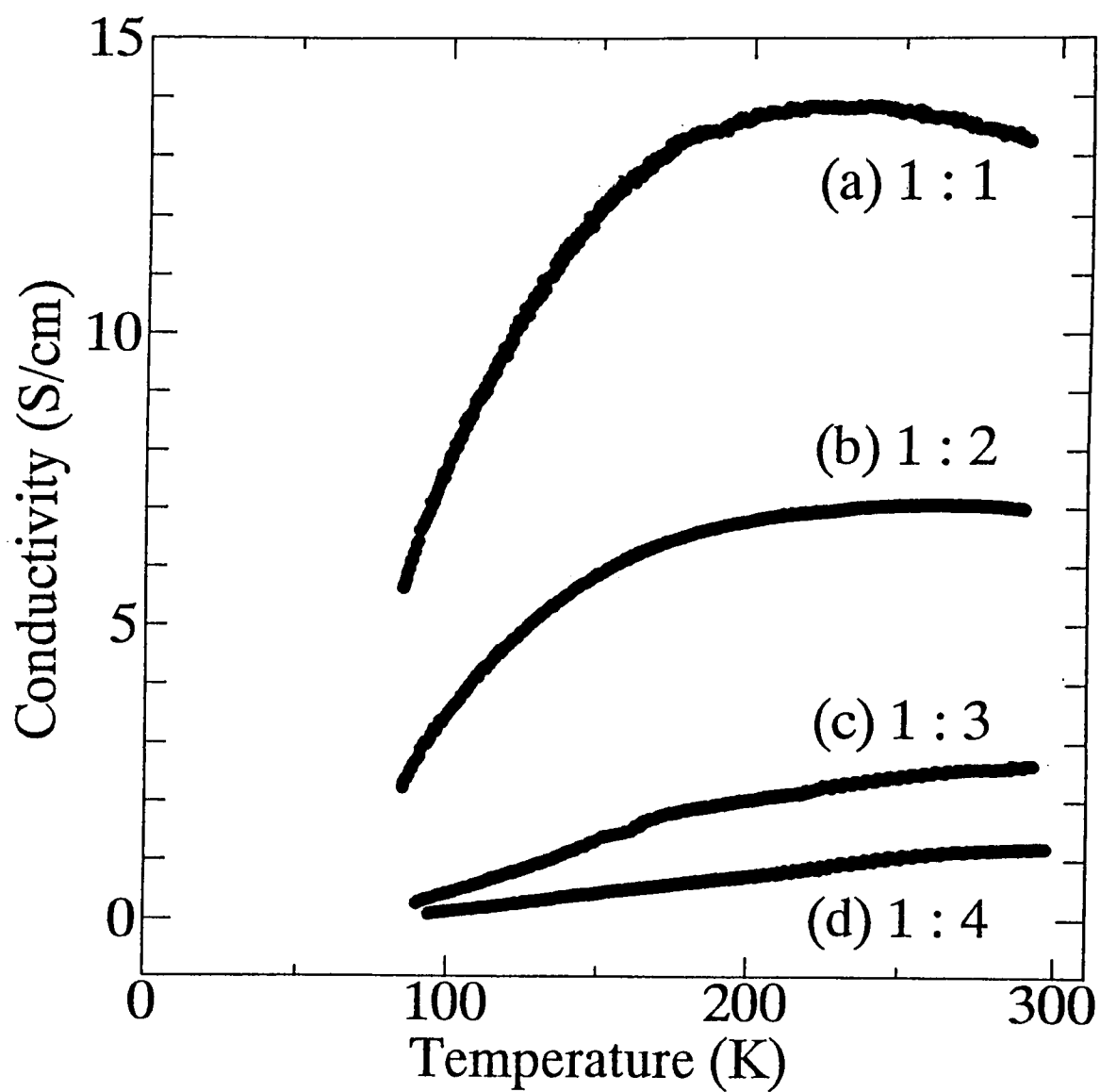


Fig. 12. Temperature dependences of the electrical conductivity for BO-C<sub>10</sub>TCNQ LB film with (a) 1 : 1 , (b) 1 : 2 and (c) 1 : 4 ratio of C<sub>10</sub>TCNQ to IA.

observed for the IA homogeneous LB film is shown in Fig. 13(b). In this case, only one diffraction peak series (Dseries) is observed, corresponding to the interplanar spacing equal to 4.9 nm. The odd-indexed peaks are stronger than the even ones indicating that IA molecules are stacked in the so-called Y-type arrangement, forming a bilayer structure as described in Ref. [14].

The observed diffraction profiles for the BO-C<sub>10</sub>TCNQ LB films (1 : X film with X = 1, 2, 4) are shown in Fig. 14. The profiles can be decomposed into four series, and a new series of peaks (C series) appeared in addition to the A, B and D series. A remarkable point is that the spacing of C series ( $d_C$ ) decreases for larger X as listed in Table 4. A probable interpretation of this is as following. During the deposition of the LB film, BO and C<sub>10</sub>TCNQ molecules form the CT complex on the water surface. However, according to the Hückel calculation, the lowest unoccupied molecular orbital of C<sub>10</sub>TCNQ is concentrated at the ends of the molecule [28]. When the charge transfer occurs, the charged orbitals tend to couple with the polarized water molecules. Moreover, the BO-C<sub>10</sub>TCNQ complex possesses unstable vacant spaces due to the long alkyl chains. Then the CT complexes formed on the water surface tend to contain water molecules around C<sub>10</sub>TCNQ resulting in the enlarged lattice spacing. The variation of the spacing of C series indicates that the CT complex tends to contain more water molecules when the amount of supporting IA molecules is smaller. Such CT complex region containing water molecules should possess disorders resulting in semiconducting characteristics. The A and B series correspond to the BO-C<sub>10</sub>TCNQ complex domain, while D series corresponds to the IA domain. The ratio of integrated intensity of the third peak of the D series ( $I_{D(3)}$ ) to the first peak of the A series ( $I_{A(1)}$ ) is listed for X = 1, 2, 4 in Table 4. A systematic growth of D series for larger X is observed as expected.

The coherence length of each periodic structure in the direction perpendicular to the

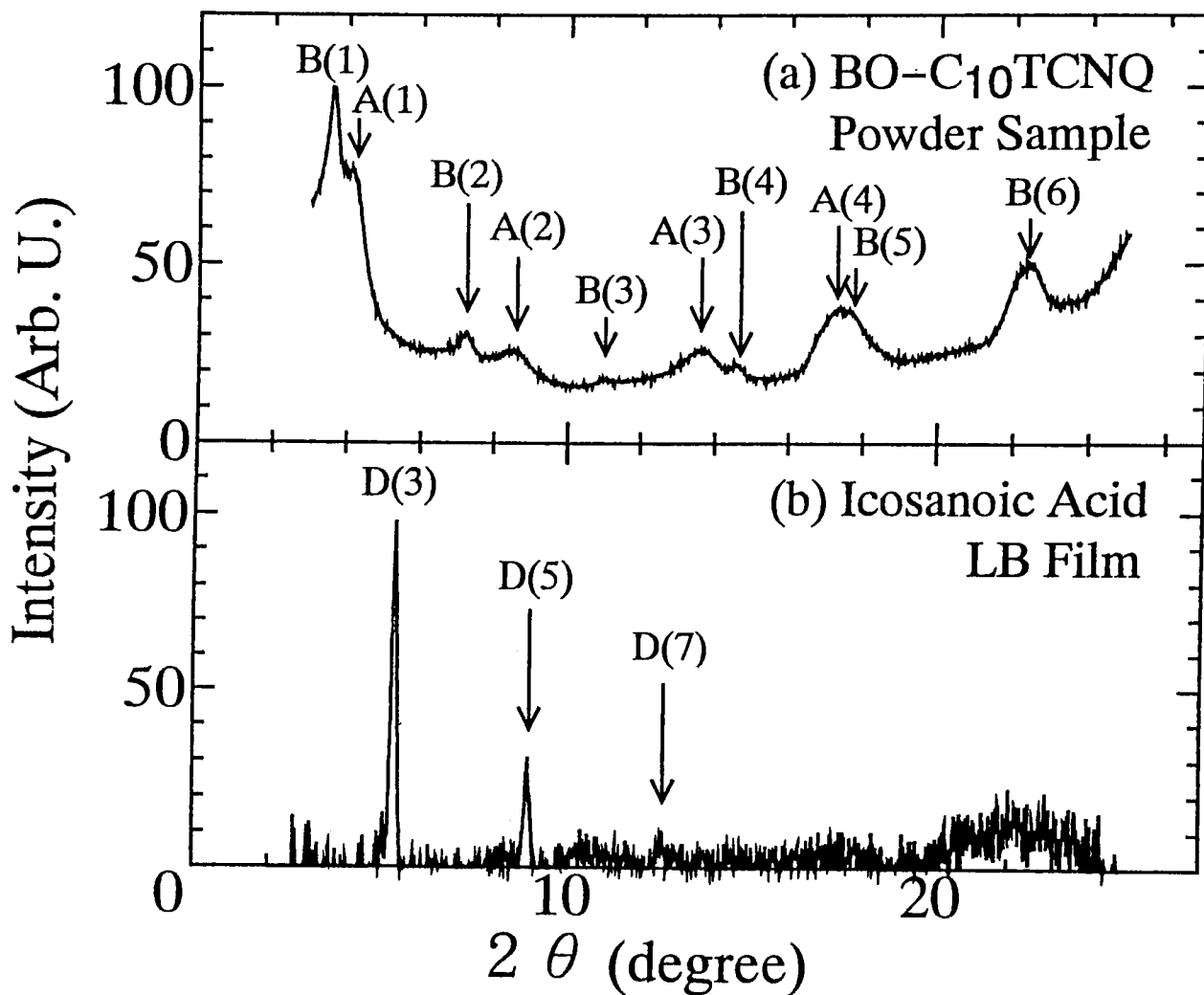


Fig. 13. X-ray diffraction profiles for (a) powder sample of BO-C<sub>10</sub>TCNQ complex and (b) homogeneous LB film of IA.



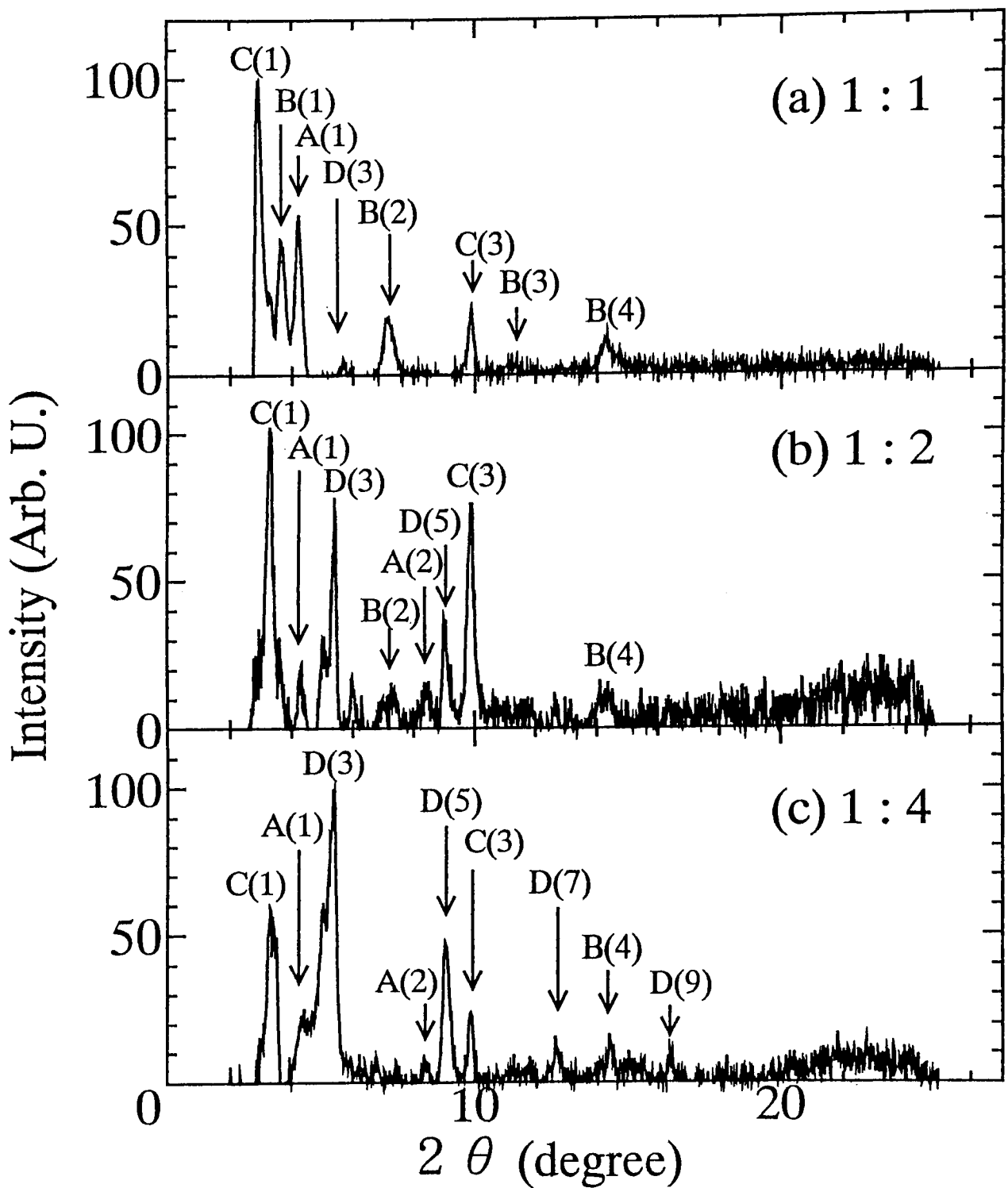


Fig. 14. X-ray diffraction profiles for BO-C<sub>10</sub>TCNQ LB film with (a) 1 : 1 , (b) 1 : 2 and (c) 1 : 4 ratio of C<sub>10</sub>TCNQ to IA.

Table 4: List of experimental parameters related to X-ray diffraction.

X	1	2	3	4
$d_C$ (nm)	3.0	2.7	–	2.6
$I_{D(3)}/I_{A(1)}$	0.096	3.2	–	7.4

film plane was estimated from the peak width for the 1 : 1 film, as  $\xi_A = 34.0$  nm ,  $\xi_B = 29.4$  nm and  $\xi_C = 36.8$  nm. Since the intensity of the D series is very small for the 1 : 1 film, the coherence length of the D series was estimated for the 1 : 2 film as  $\xi_D = 40.1$  nm. Considering the thickness of the monolayer on the water surface (2.5 nm), these values indicate that the same molecular stacking is repeated more than 10 times on the average within each domain. This indicates that the molecular arrangements within each layer is affected by the preceding layer: the molecular arrangements in the LB film are not only self-assembled within the layer but also correlated in the interlayer direction probably by migration during the deposition. This is possible because the deposition of LB film is carried out in a wet environment.

### 3.3 Electron spin resonance

The ESR spectra for the 1 : 1 film measured at X-band (9.4 GHz) at 10 K with different configuration of dc magnetic field are shown in Fig. 15. At this temperature, the anisotropy of the spectra is most emphasized. The spectrum shown in Fig. 15(a) indicates that there exist two kinds of spin species. They are decomposed by least-square fitting method by assuming the Lorentzian line shapes [29]. When the dc magnetic field is parallel to the film plane, the separation of the peaks becomes difficult especially at low temperature due to the nearly equal  $g$ -values. This anisotropy strongly indicates that the CT complex molecules are well oriented within the film [30].

The decomposition of peaks were carried out for the 1 :  $X$  films ( $X = 1, 2, 4$ ) with

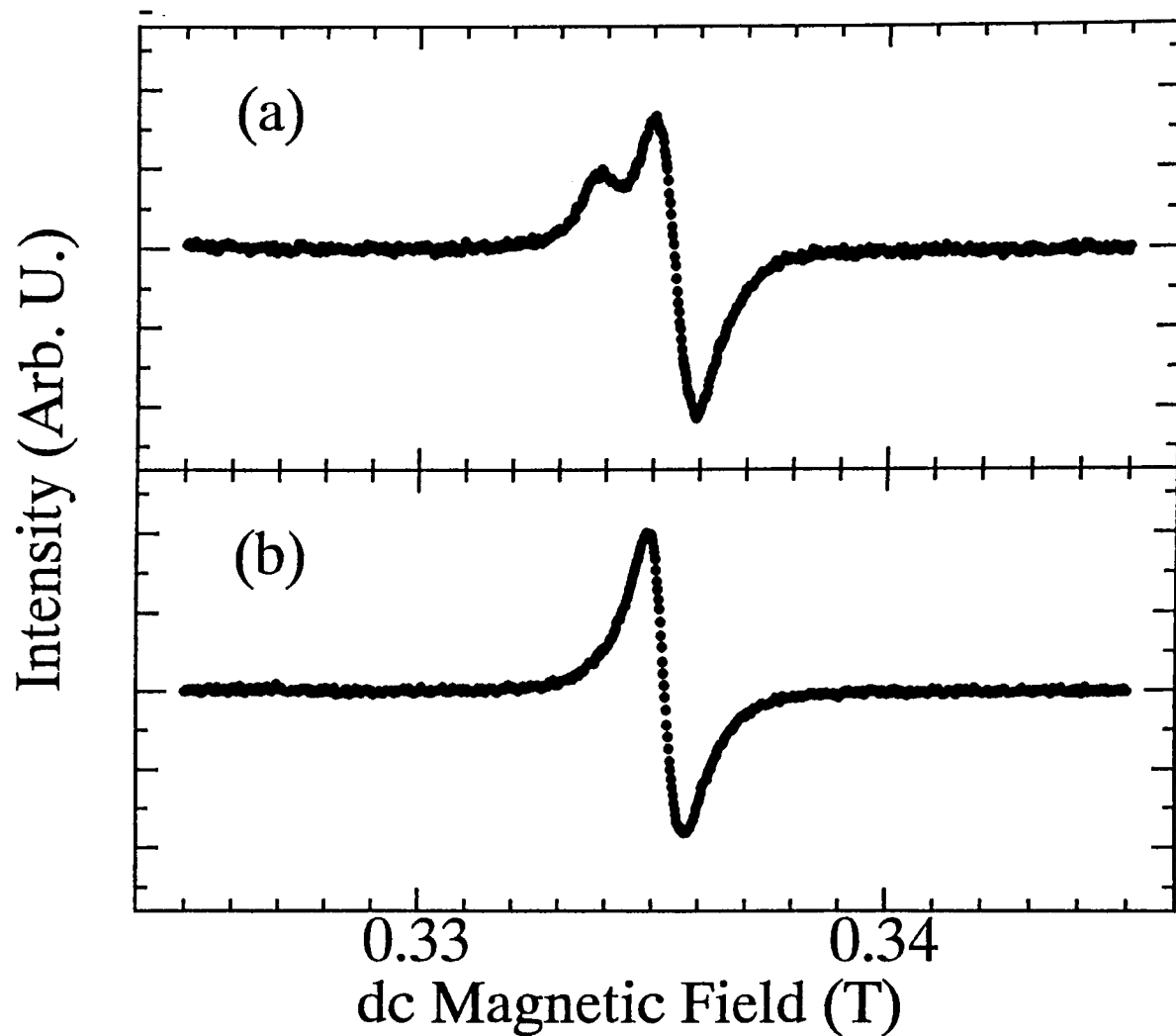


Fig. 15. ESR spectra for BO-C<sub>10</sub>TCNQ LB film with 1 : 1 ratio of C<sub>10</sub>TCNQ to IA at the X-band at 10 K with dc magnetic field (a) perpendicular and (b) parallel to the film plane.

dc magnetic field perpendicular to the film plane. The temperature dependences of the  $g$ -values are shown in Fig. 16. The species with larger  $g$ -value (species I) is attributed to BO, while that with smaller  $g$ -value (species II) is attributed to C<sub>10</sub>TCNQ after Ikegami *et al.* [29]. For the species I, the  $g$ -value slightly increases with decreasing temperature, while for the species II, the  $g$ -value is constant in the whole temperature range. The room-temperature  $g$ -values for the species I ( $g_I$ ) and those for the species II ( $g_{II}$ ) are listed in Table 5. Since the variation of the  $g$ -values are within the error, there is no clear correlation between the  $g$ -values and  $X$ .

The temperature dependences of the spin susceptibility ( $\chi_s$ ) of the 1 :  $X$  film ( $X=1, 2, 4$ ) are shown in Fig. 17, where  $\chi_s$  is normalized by the value of species I at 290 K ( $\chi_I(290\text{K})$ ). For the species I, the temperature-independent, Pauli-like  $\chi_s$  is observed above 50 K. The rapid increase of  $\chi_s$  below that temperature is ascribable to a Curie component due to the coexisting localized part. The temperature dependences of  $\chi_s$  for the species II shows Curie-like behavior as expected for localized spins on C<sub>10</sub>TCNQ.

The temperature dependences of the line width  $\Gamma$  of the 1 :  $X$  film ( $X=1, 2, 4$ ) are shown in Fig. 18. The line width of the species I decreases with decreasing temperature. For 1 : 2 film and 1 : 4 film,  $\Gamma$  seems to have local maximums at 120 K and 160 K, respectively, but this is probably due to the uncertainty in peak decomposition. The room-temperature line width for the species I ( $\Gamma_I$ ) and those for the species II ( $\Gamma_{II}$ ) are listed in Table 5. There is no clear correlation between the line width and  $X$ .

The results of ESR measurements imply the presence of metallic domains above 50 K. The temperature dependence of the line width is ascribable to the Elliott mechanism [31] described below. Considering the spin-orbit interaction, the electron-phonon interaction possesses finite matrix elements between opposite spin states, and the spin relaxation of the conduction electrons due to the phonon scattering occurs through such spin-orbit coupling.

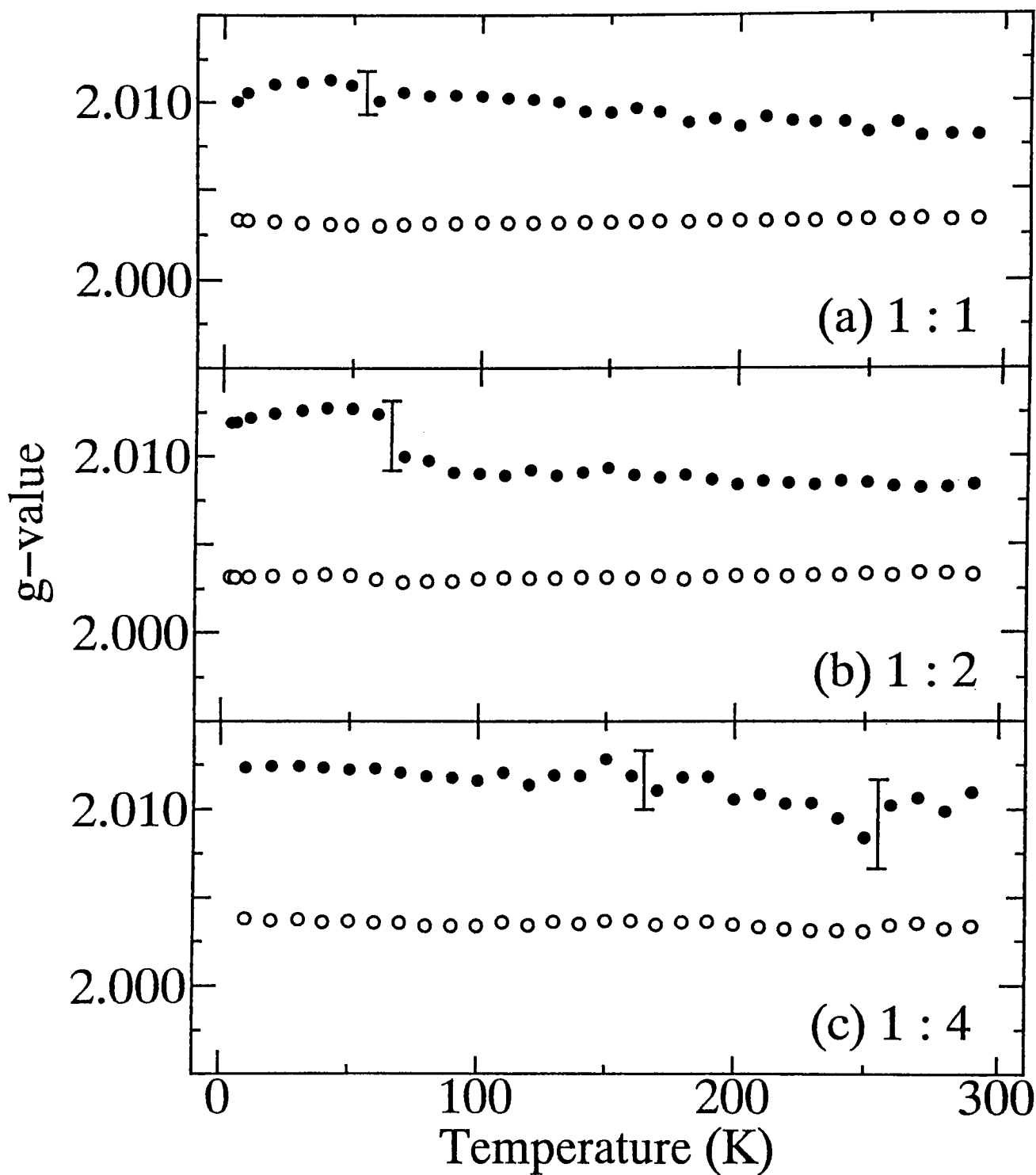


Fig. 16. Temperature dependences of the g-values for BO-C<sub>10</sub>TCNQ LB film with (a) 1 : 1, (b) 1 : 2 and (c) 1 : 4 ratio of C<sub>10</sub>TCNQ to IA. Closed circles denote the data for the species I and open circles for the species II.

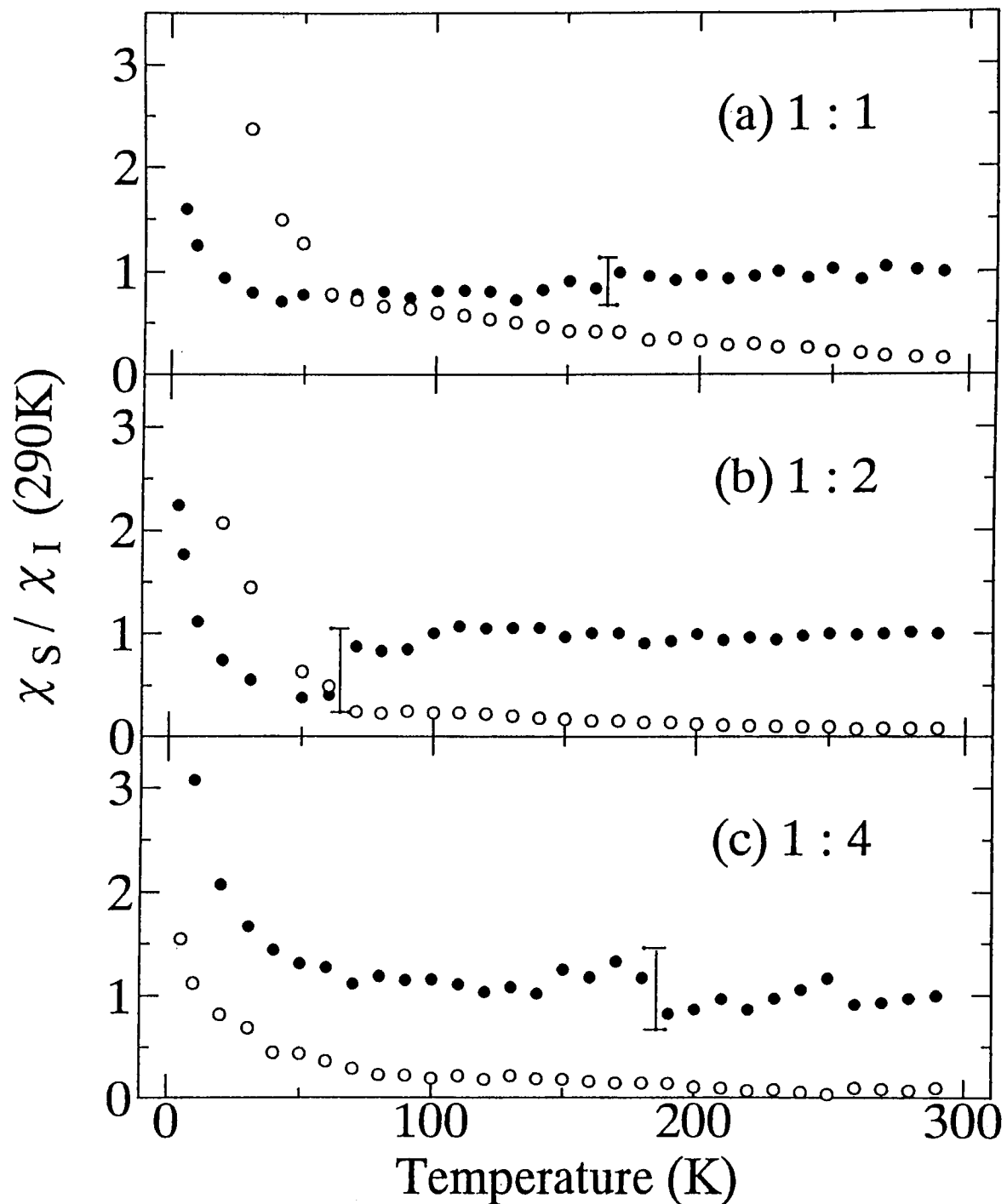


Fig. 17. Temperature dependences of the spin susceptibility for BO-C<sub>10</sub>TCNQ LB film with (a) 1 : 1, (b) 1 : 2 and (c) 1 : 4 ratio of C<sub>10</sub>TCNQ to IA. Closed circles denote the data for the species I and open circles for the species II.

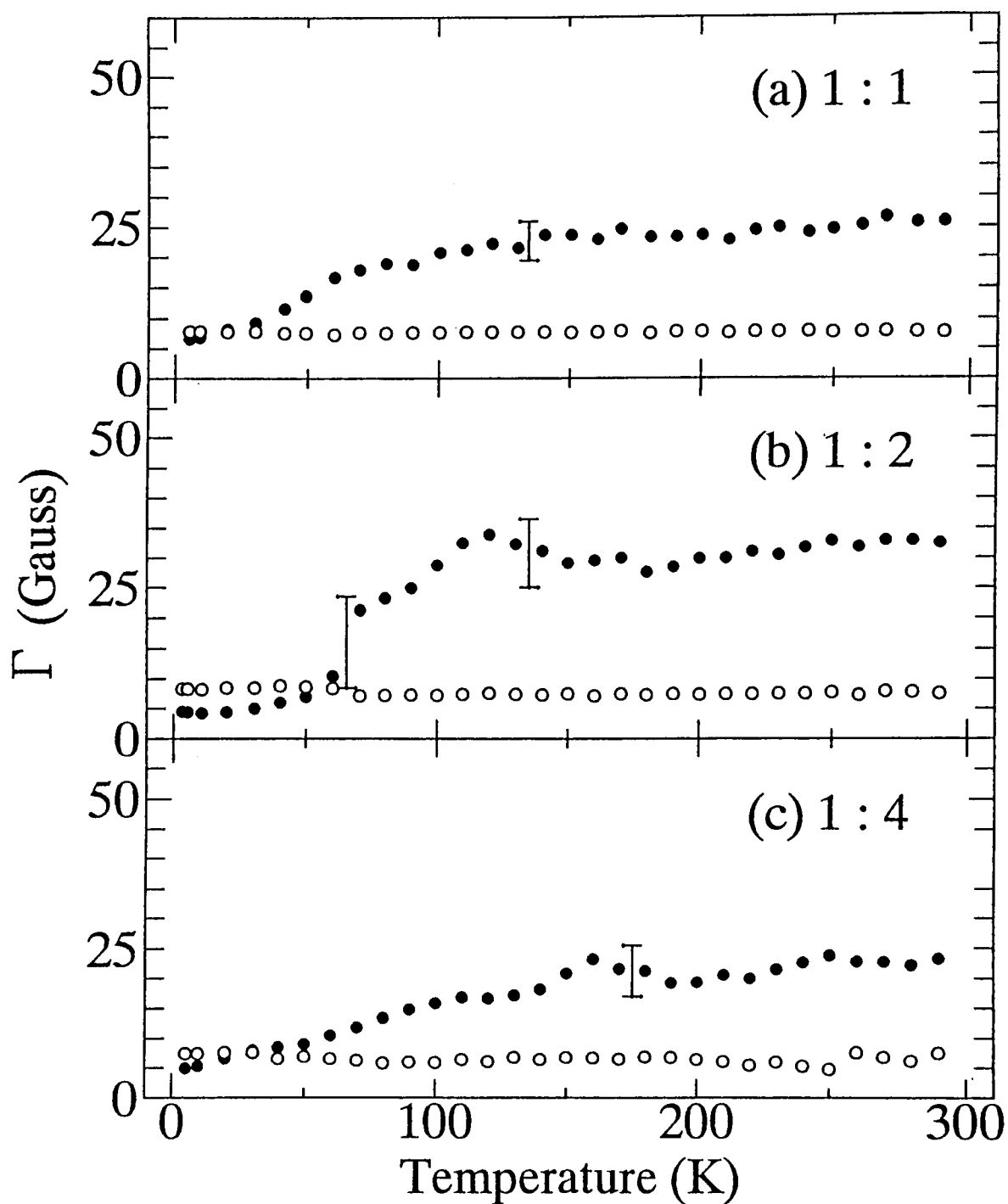


Fig. 18. Temperature dependences of the ESR line width for BO-C<sub>10</sub>TCNQ LB film with (a) 1 : 1 , (b) 1 : 2 and (c) 1 : 4 ratio of C<sub>10</sub>TCNQ to IA. Closed circles denote the data for the species I and open circles for the species II.

As a result, the spin-relaxation time ( $\tau_S$ ) and the relaxation time for resistivity ( $\tau_R$ ) are not independent but have a certain relationship such as

$$\tau_S \propto \frac{\tau_R}{(g-2)^2}. \quad (10)$$

Here,  $\tau_S$  corresponds to the spin-lattice relaxation time ( $\tau_1$ ) and the line width is proportional to the inverse of the spin-spin relaxation time ( $\tau_2$ ). Assuming  $\tau_S = \tau_1 = \tau_2$ , because the difference of the local field should be averaged out and  $\tau_2$  is dominated by  $\tau_1$  for conduction electrons, the temperature dependence of the line width is represented by the temperature dependence of the resistivity, although it is also affected by the shift of the  $g$ -value ( $g-2$ ). As a result, a decrease of  $\Gamma$  with decreasing temperature is expected for metals. The relatively large  $g$ -value, the temperature-independent  $\chi_s$  and the decrease of  $\Gamma$  with decreasing temperature for the BO-C<sub>10</sub>TCNQ LB films support the presence of metallic domains above 50 K. The  $g$ -values and line widths are almost independent on  $X$ , indicating that metallic domains exist irrespective of  $X$ . The localized spins giving the Curie-like behavior at low temperature is ascribable to the disordered CT complex domains containing water molecules. The ratio of localized spins and conduction electrons depends on  $X$  as observed in the temperature dependence of  $\chi_s$  for the species I.

According to the power dependence of the ESR intensity, we found that the signals for the species I is free form saturation in a whole temperature range, while those for the species II are suppressed due to the saturation. Then we carry out quantitative analysis only for the species I. In order to estimate the ratio of localized spins on BO molecules, we fitted the temperature dependence of  $\chi_s$  with a simple sum of Pauli susceptibility and Curie susceptibility for the species I,

$$\chi_s \propto \frac{1}{2}g_I^2\mu_B^2 D(\varepsilon_F) + \frac{N_c^B g_I^2 \mu_B^2}{4kT}, \quad (11)$$

where  $D(\varepsilon_F)$  is the density of states at the Fermi surface,  $N_c^B$  the number density of Curie



Table 5: List of experimental parameters related to ESR.

X	1	2	3	4
$g_I(290K)$	2.008	2.008	–	2.011
$g_{II}(290K)$	2.004	2.004	–	2.004
$\Gamma_I(290K)$	26.0	32.5	–	23.3
$\Gamma_{II}(290K)$	7.8	7.6	–	7.6
$N_c^B/(kD(\varepsilon_F))$ (K)	8.01	9.51	–	34.8

spins coming from BO,  $\mu_B$  the Bohr magneton,  $k$  the Boltzman constant. The ratio of  $N_c^B$  to  $D(\varepsilon_F)$  in the unit of  $k$  is listed in Table 6, which is related to the amount of localized spins of BO region. A systematic increase of the ratio represents the domain size as described below. In the formation of LB film, the CT complex are scattered all over the film resulting in the smaller domain size for larger  $X$ . When the domain size become smaller, the spins tend to be isolated from each other and the number of isolated spins increases.

### 3.4 Atomic force microscopy

The AFM topographic images for the 1 :  $X$  film ( $X = 1, 2, 4$ ) in the scanning areas of  $5 \times 5 \mu\text{m}^2$  and  $10 \times 10 \mu\text{m}^2$  are shown in Fig. 19. The domains of constituent molecules are clearly observed, although the molecular arrangement within the domains could not be resolved in these samples. The images shown in Fig. 19 indicate that the amount of needle-like domains increase with decreasing  $X$ , implying that the domains of the CT complex are apt to extend directionally. This is supported by another experiment. For 3-layer BO-(MeO)<sub>2</sub>TCNQ LB film deposited on graphite, the AFM measurements were carried out in the scanning area of  $2 \times 2 \mu\text{m}^2$  by the simultaneous current measurements mode with bias voltage of 0.01 V. The results are also shown in Fig. 19, where bright region represents the conductive region, indicating that the shape of the CT complex region is needle-like. The typical size of the domains is  $300 \times 50 \text{ nm}^2$ . Although the anion in the CT complex is different in this case, similar properties are expected for BO-C<sub>10</sub>TCNQ.

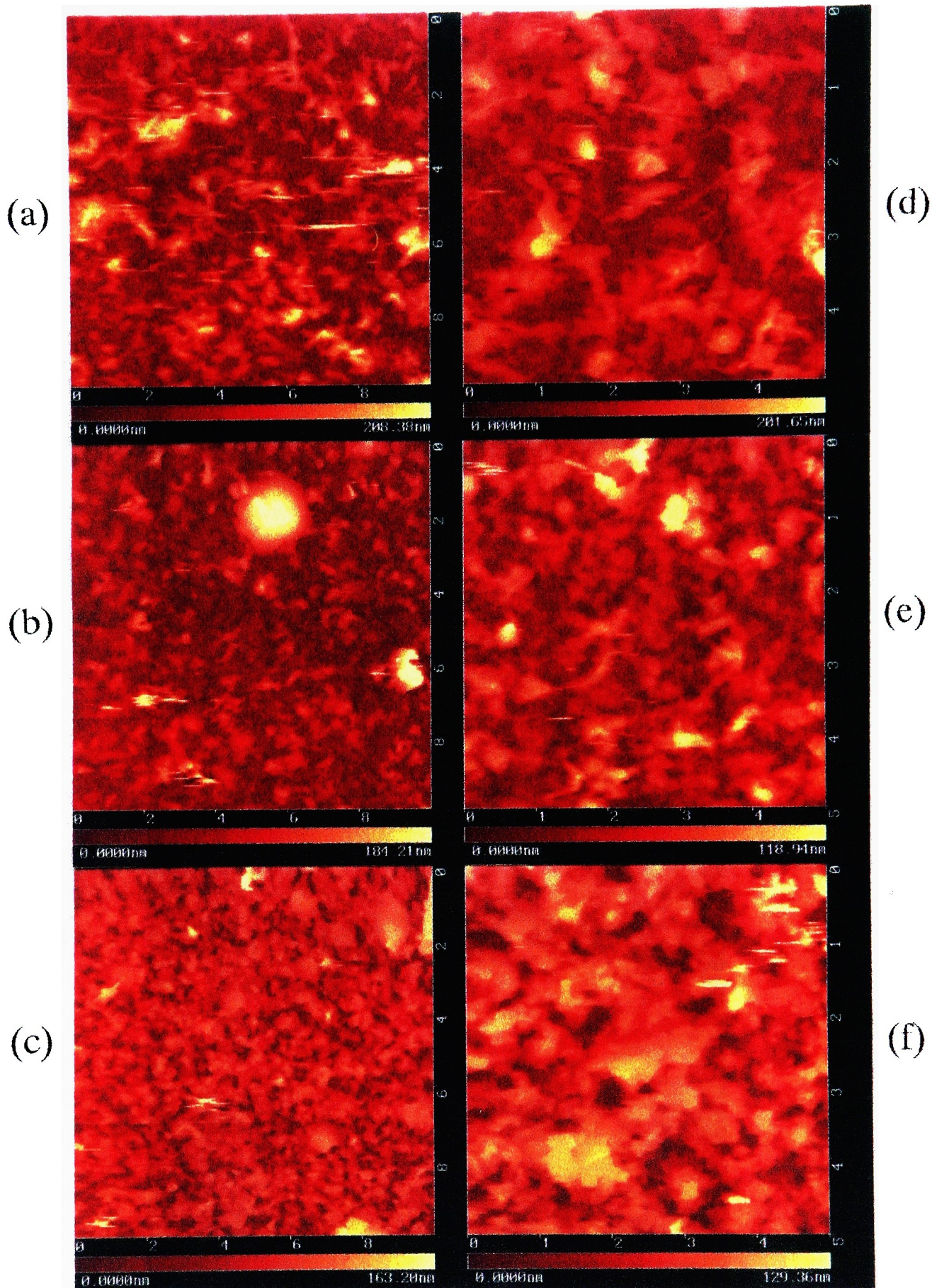
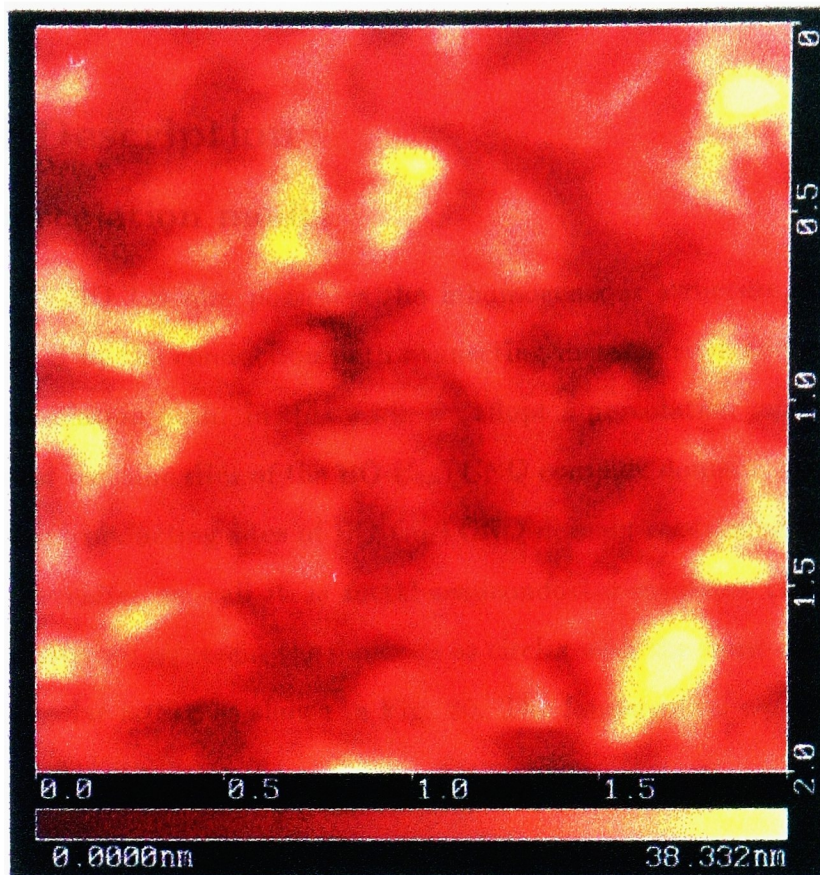


Fig. 19. AFM topographic images in the scanning area of  $10 \times 10 \mu\text{m}^2$  for BO- $\text{C}_{10}\text{TCNQ}$  LB film with (a) 1 : 1 , (b) 1 : 2 and (c) 1 : 4 ratio of  $\text{C}_{10}\text{TCNQ}$  to IA, and those in the scanning area of  $5 \times 5 \mu\text{m}^2$  for BO- $\text{C}_{10}\text{TCNQ}$  LB film with (d) 1 : 1 , (e) 1 : 2 and (f) 1 : 4 ratio of  $\text{C}_{10}\text{TCNQ}$  to IA.

(g)



(h)

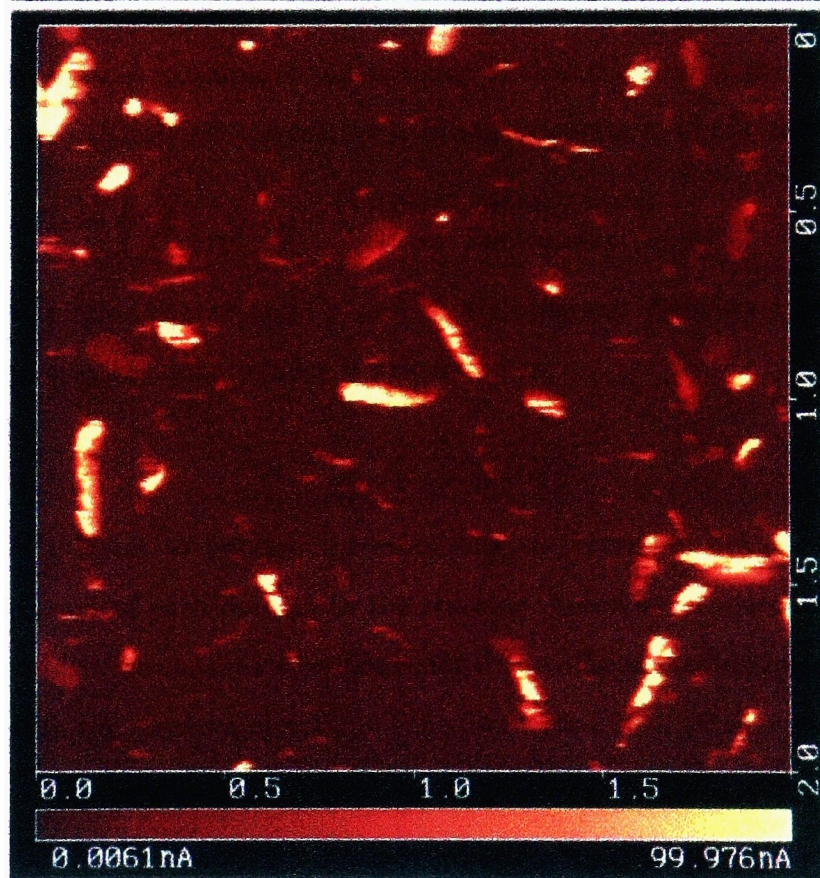


Fig. 19. (g) AFM topographic image and (h) current image in the scanning area of  $2 \times 2 \mu\text{m}^2$  for 3-layer BO-(MeO)<sub>2</sub>TCNQ LB film on graphite.

## 4 Model Description

### 4.1 MSI percolation model

Since BO-C<sub>10</sub>TCNQ LB film possesses the inhomogeneous structure, the conduction should be influenced by the conduction path connecting metallic sites and semiconducting sites, *i. e.*, the percolation path. In this work, we adopt a percolation model consisting of three kinds of sites: metallic sites of the BO-C<sub>10</sub>TCNQ complex domain, insulating sites of IA domain and semiconducting sites of BO-C<sub>10</sub>TCNQ domain containing water molecules and disorders. Hereafter we call it as metal-semiconductor-insulator (MSI) percolation model. For simplicity, we represent the domains as circles with the same size arranged in a close-packed triangular lattice as shown in Fig. 20. The fundamental equation is given by

$$\sum_j C_{ij}(V_j - V_i) = 0, \quad (12)$$

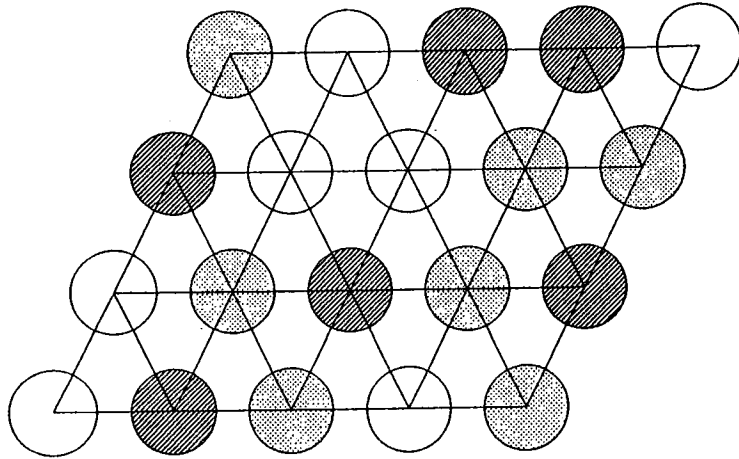
where  $V_i$  is the voltage at each site and  $C_{ij}$  is the conductance of the bond connecting  $i$  and  $j$  sites. The physical meaning of the equation is that the sum of the currents coming into each site is zero (Kirchhoff current law). In our calculation,  $C_{ij}$  is assumed to be

$$C_{ij} = \begin{cases} \frac{C_m}{T} & \text{(between metallic sites)} \\ C_s \exp(-\frac{E}{T}) & \text{(between semiconducting sites)} \end{cases}, \quad (13)$$

where  $E$  is the activation energy and  $C_m$  and  $C_s$  are constant. Between a metallic site and a semiconducting site, the conductance is calculated as,

$$C_{ij} = \frac{1}{\frac{T}{2C_m} + \frac{1}{2C_s} \exp(\frac{E}{T})} \quad (14)$$

In other cases,  $C_{ij}$  is set to be zero corresponding to insulating behavior. Taking into account the coherence of each domain in the stacking direction estimated from the X-ray diffraction peak width, we consider two-dimensional percolation conduction and neglect the percolation effect in the stacking direction of the film. Then  $20 \times 20$  sites were used for the



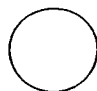
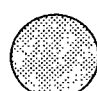

-  Insulating Site
-  Metallic Site
-  Semiconducting Site

Fig. 20. MSI percolation model representing a random arrangement of metallic, semiconducting and insulating sites.

numerical calculation. The metallic sites and semiconducting sites are selected randomly according to the fractions  $p_m$  and  $p_s$ , respectively. The conductance of the random network is obtained by setting the voltage at each site on one end equal to zero, assigning a constant voltage to all sites on the opposite end, and solving Eq. 12 numerically to obtain the current flow between them [32]. Cyclic boundary conditions are imposed in the direction perpendicular to the applied voltage. For the simulation of the electrical conductivity, we have 5 parameters, such as  $p_m$ ,  $p_s$ ,  $C_m$ ,  $C_s$ ,  $E$ . However, from physical point of view, it is useful to define a new set of parameters,

$$\begin{cases} p_1 = p_m + p_s \\ p_2 = p_m / (p_s + p_m) \\ C_{ms} = C_m / C_s \\ E \end{cases}, \quad (15)$$

where  $p_1$  corresponds to the fraction of CT complex within the film,  $p_2$  the fraction of metallic CT complex within the CT complex region. Assuming that the temperature dependence of the conductivity is not affected by absolute values of  $C_m$  and  $C_s$ , we study the effect of their ratio  $C_{ms}$ . The temperature dependence of the conductivity calculated for various values of  $C_{ms}$  with  $p_1 = 0.8$ ,  $p_2 = 0.4$ ,  $E = 100$  K is shown in Fig. 21(a). The results show that the conductivity increases and the temperature with the maximum conductance shifts toward the higher temperature for larger  $C_{ms}$ . This means that the macroscopic metallic temperature dependence is suppressed when the conductivity of the metallic region becomes larger. It sounds somewhat strange, but understandable considering that the conductivity is dominated by semiconducting region when the conductivity of the metallic region is large enough. The conductivity calculated for various values of  $E$  with  $p_1 = 0.8$ ,  $p_2 = 0.4$ ,  $C_{ms} = 1000$  are shown in Fig. 21(b). The results show that the conductivity increases and the temperature with the maximum conductance shifts toward lower temperature for smaller  $E$ . Now considering the effects of these parameters on the temperature with the maximum conductance, we have to check whether the temperature dependence changes or

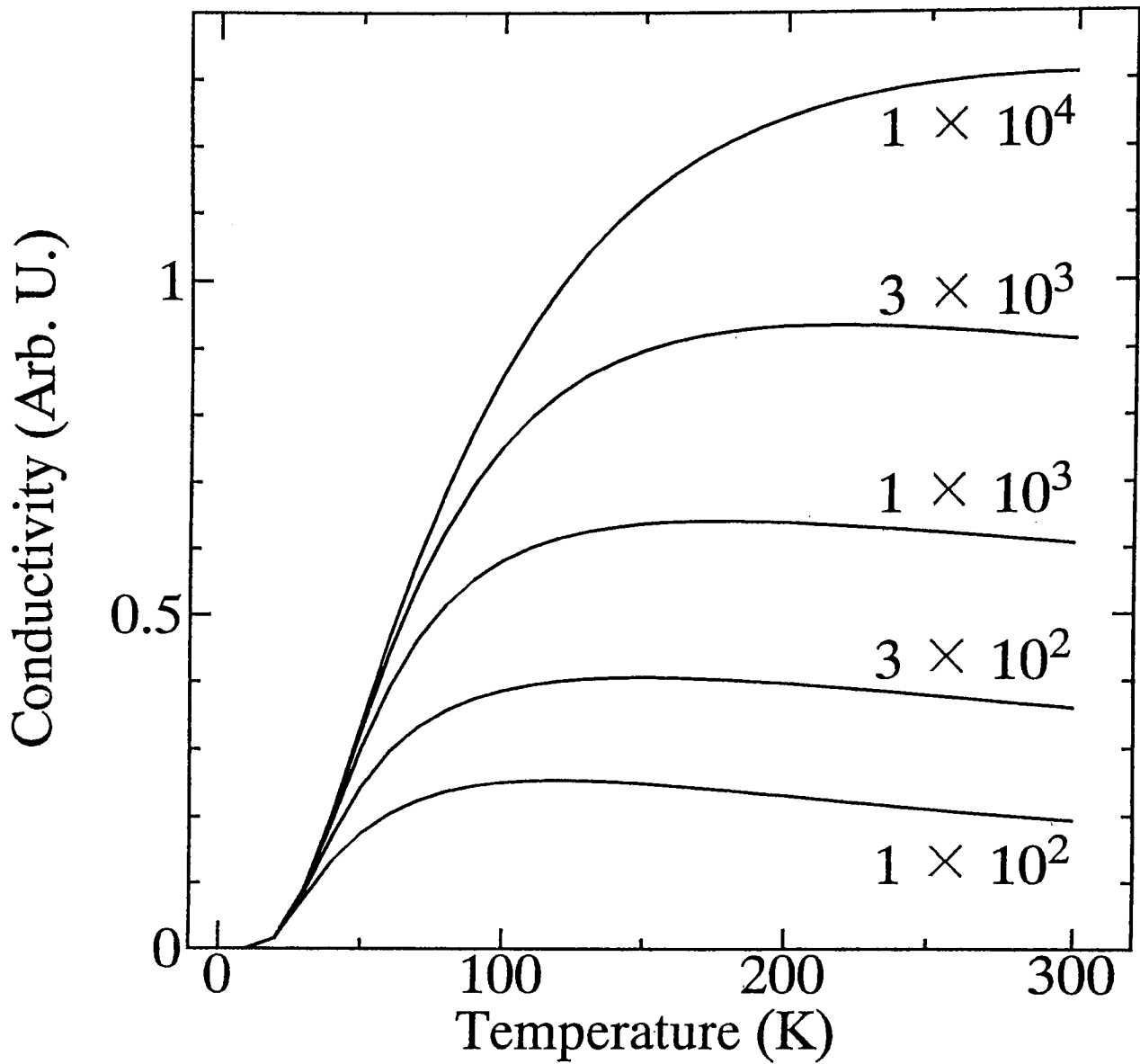


Fig. 21(a). Temperature dependences of the electrical conductivity calculated for various values of  $C_{ms}$  based on the two-dimensional MSI percolation model with  $p_1 = 0.8$ ,  $p_2 = 0.4$ ,  $E = 100$  K.

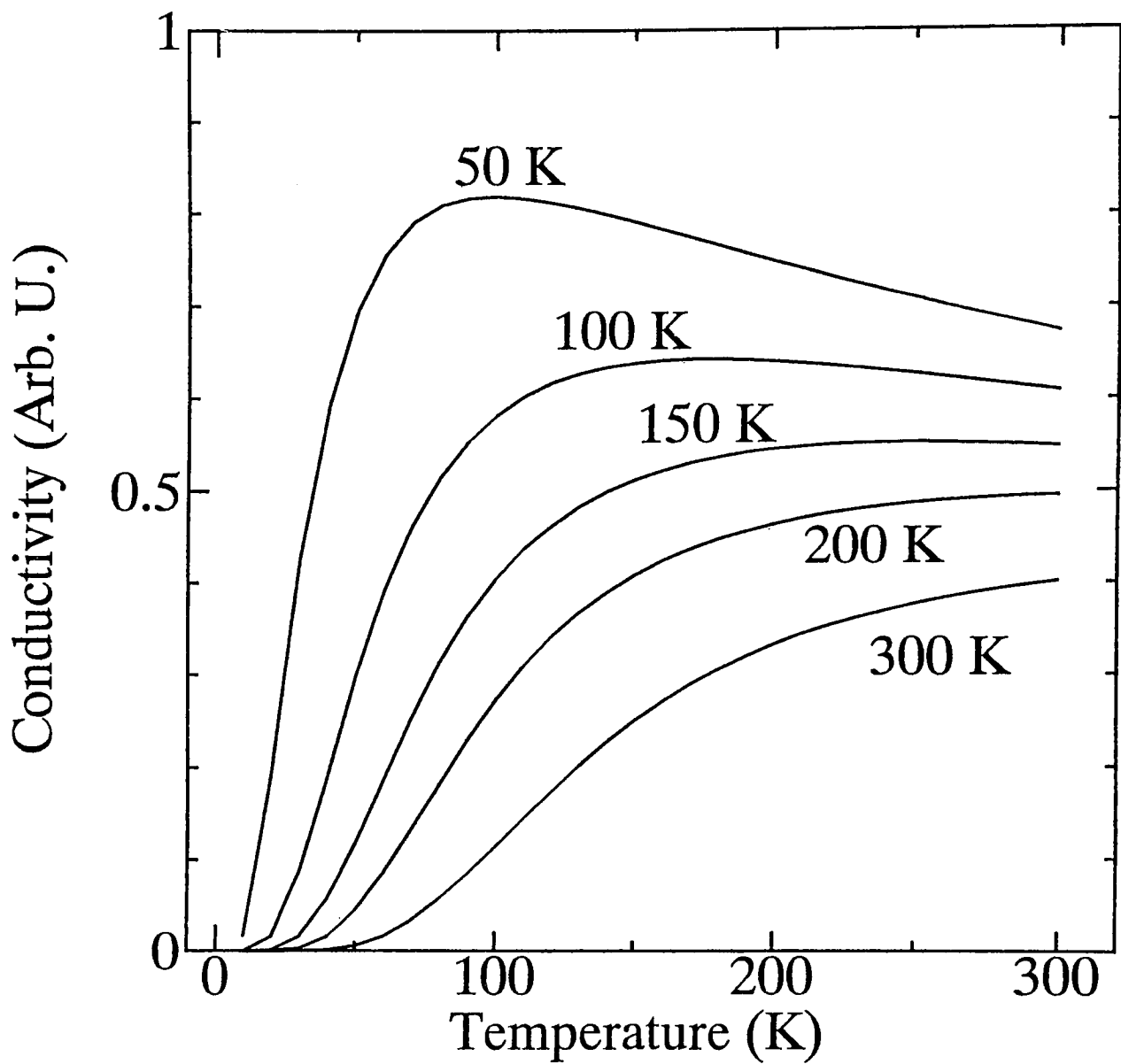


Fig. 21(b). Temperature dependences of the electrical conductivity calculated for various values of  $E$  based on the two-dimensional MSI percolation model with  $p_1 = 0.8$ ,  $p_2 = 0.4$ ,  $C_{ms} = 1000$ .



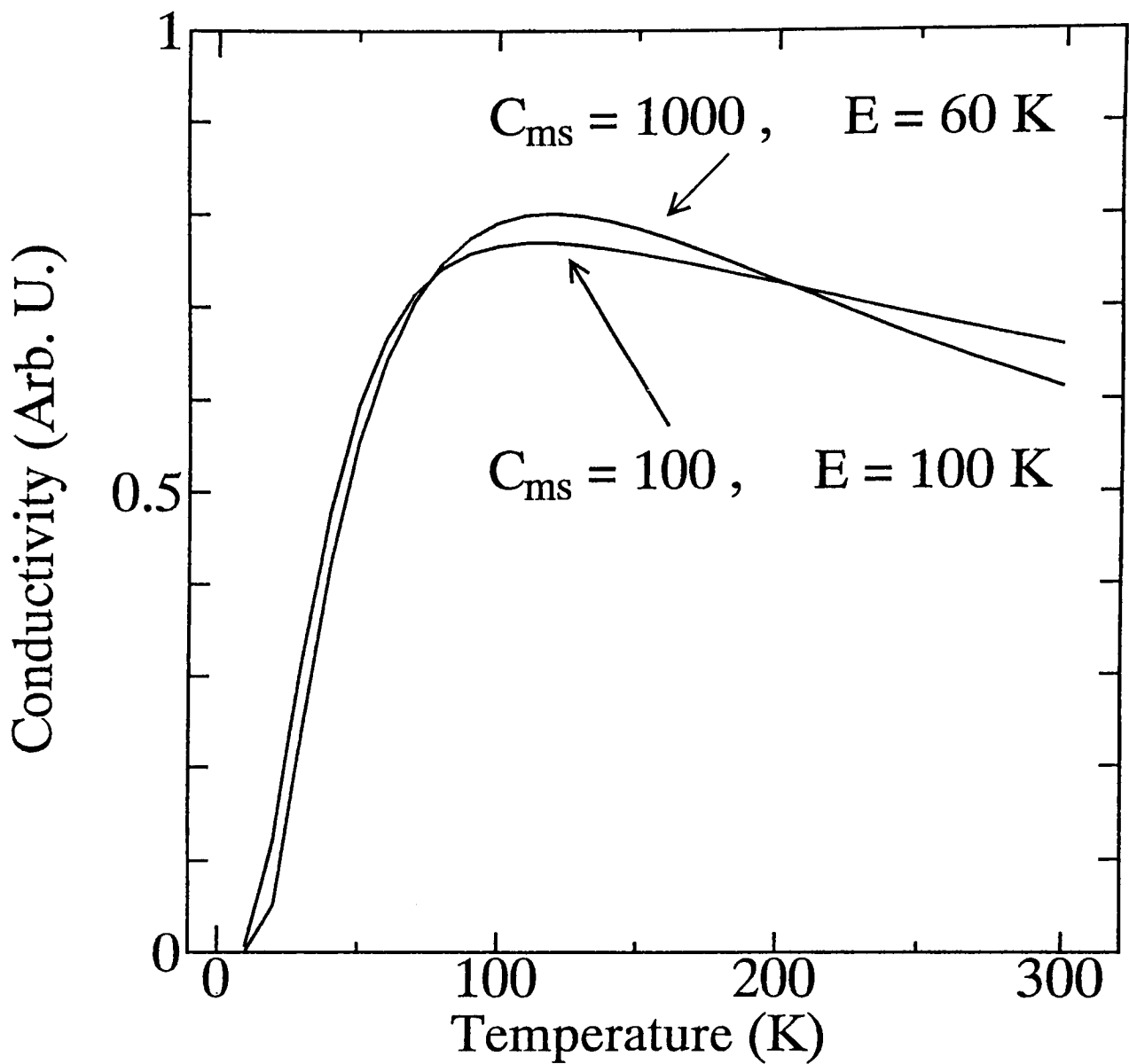


Fig. 21(c). Temperature dependences of the electrical conductivity calculated for  $C_{ms} = 1000$ ,  $E = 60 \text{ K}$  and for  $C_{ms} = 100$ ,  $E = 100 \text{ K}$  based on the two-dimensional MSI percolation model with  $p_1 = 0.8$ ,  $p_2 = 0.4$ .

not, if we use a larger value of  $C_{m,s}$  and a smaller value of  $E$ . The results calculated with  $C_{m,s} = 1000$ ,  $E = 60$  K and  $C_{m,s} = 100$ ,  $E = 100$  K are shown in appropriate scales in Fig. 21(c). Apparently, the peak become sharper for smaller  $E$ , and we can determine both  $C_{m,s}$  and  $E$  if the values of  $p_1$  and  $p_2$  are given.

## 4.2 Modified 2D MSI percolation model

For the calculation of the conductivity, we have to estimate the values of  $p_1$  and  $p_2$ . Considering the area of one BO molecule within the conductive layer ( $0.2 \text{ nm}^2$ ) [33], that of one IA molecule within the monolayer on the water surface ( $0.2 \text{ nm}^2$ ) [34] and the number ratio of BO to IA (2.5 : 1), the values of  $p_1$  can be calculated by

$$p_1^{th} = \frac{2.5}{2.5 + X}, \quad (16)$$

which are listed in Table 6. According to the general theory of the percolation [35], the percolation threshold of the two-dimensional close-packed triangular lattice ( $p_c^{2D}$ ) is equal to 0.5. However, in the case of  $X = 4$ , the conductive LB film is obtained in spite of  $p_1 < p_c^{2D}$ , indicating that the effective dimension of the present system is more than two. This is partly due to the percolation path formed in the stacking direction of the LB film because the coherence length of each domain is a little smaller than the film thickness. In order to study the effect of dimensionality, we numerically calculated the site occupancy ( $p$ ) dependence of the conductance for two-dimensional close-packed lattice as shown by solid circles in Fig. 22, where the conductance is normalized by the value for  $p = 1$ . Above the percolation threshold, the behavior of the conductance is approximately represented by a parabola,

$$\sigma(p) = ap^2 + bp + c, \quad (17)$$

with  $a = 1.48$ ,  $b = -0.25$  and  $c = -0.23$  as shown by solid line in Fig. 22. Using  $p_1^{th}$  for the value of  $p$ , the experimental data for the BO-C<sub>10</sub>TCNQ LB film are also fitted by a

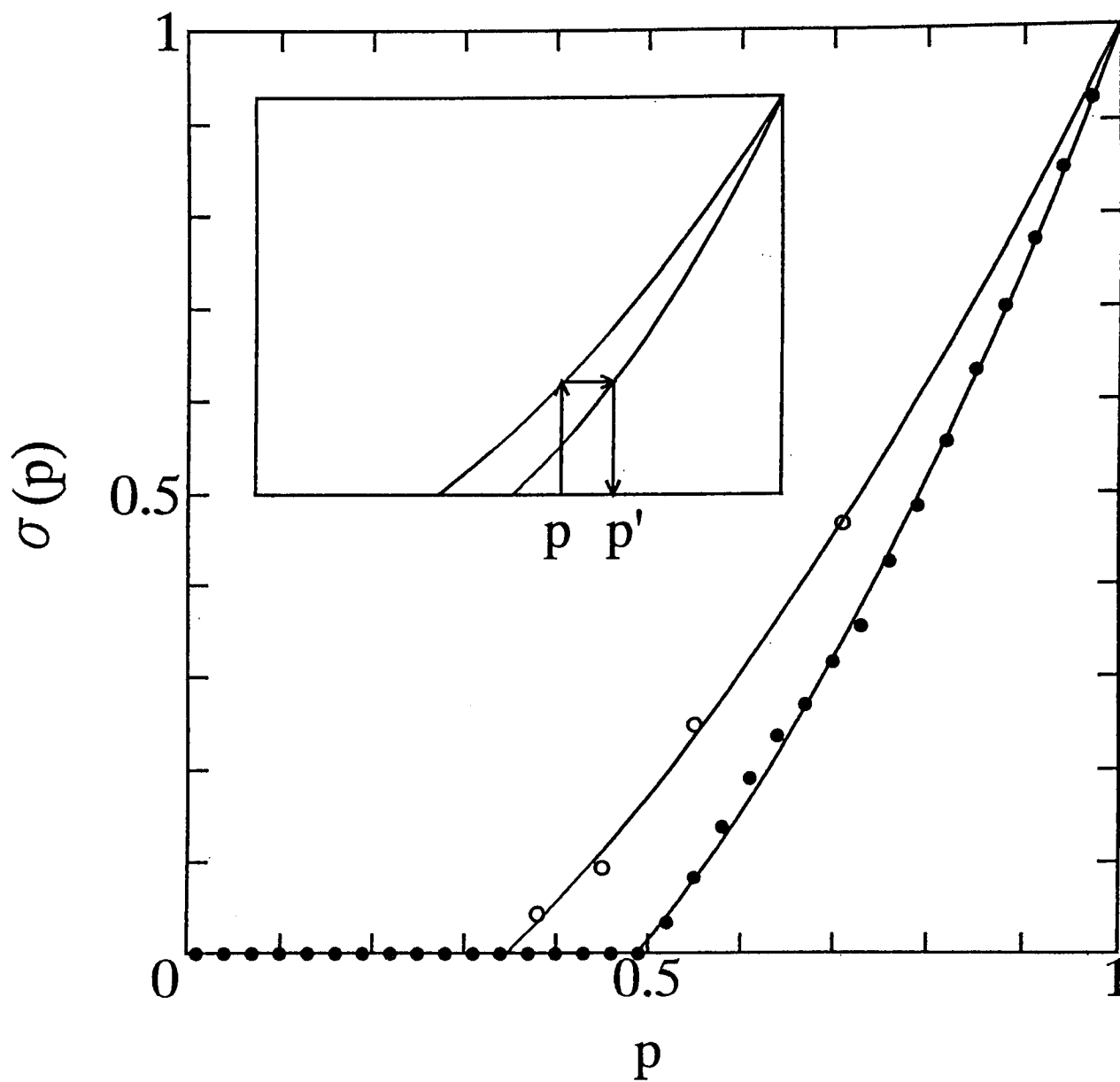


Fig. 22. Site occupancy dependence of the conductance calculated for the two-dimensional close-packed lattice (solid circles) and experimental data for the BO-C<sub>10</sub>TCNQ LB film (open circles), where the conductance is normalized by the value for  $p = 1$ . Solid lines are results of the fitting. Transformation from  $p$  to  $p'$  is illustrated schematically in the inset.

parabola,

$$\sigma(p) = a'p^2 + b'p + c', \quad (18)$$

with  $a' = 0.84$ ,  $b' = 0.41$ ,  $c' = -0.24$  as shown by open circles and solid line in Fig. 22, where the conductance is also normalized by the value for  $p = 1$ . This result indicates that the percolation threshold is equal to 0.35 in the present system. This is consistent with the fact that the conductive film could not be obtained for  $X = 6$ , which corresponds to  $p = 0.29$ , while conductive film was obtained for  $X = 4$ , which corresponds to  $p = 0.38$ . Concerning the percolation conduction, the threshold changes with dimensionality [35]. The dimension ( $D$ ) dependence of the percolation threshold ( $p_c$ ) for close-packed lattice is shown by solid circles in Fig. 23. It is useful to define an effective dimension for percolation with a relationship expressed by,

$$p_c = \frac{1}{(D-1)^2 + 1} \quad (D \geq 1), \quad (19)$$

which is shown by solid line in Fig. 23. The value of  $p_c$  defined here tends to zero for higher dimension as expected from physical picture. Based on this, the estimated effective dimension of the BO-C<sub>10</sub>TCNQ LB film is 2.4 as shown by the open circle in Fig. 23. Then, we have to calculate the conductance based on the 2.4-dimensional percolation path. However, the same value of the conductance is obtained from the calculation based on the two-dimensional percolation path using a modified site occupancy  $p'$  defined by

$$\sigma^{2.4D}(p) = \sigma^{2D}(p'), \quad (20)$$

where  $\sigma^{2.4D}$  and  $\sigma^{2D}$  are the normalized conductance for 2.4-dimension and two-dimension, respectively. The transformation from  $p$  to  $p'$  is illustrated schematically in the inset of the Fig. 22. Using the approximate expressions (17) and (18), the transformation is represented

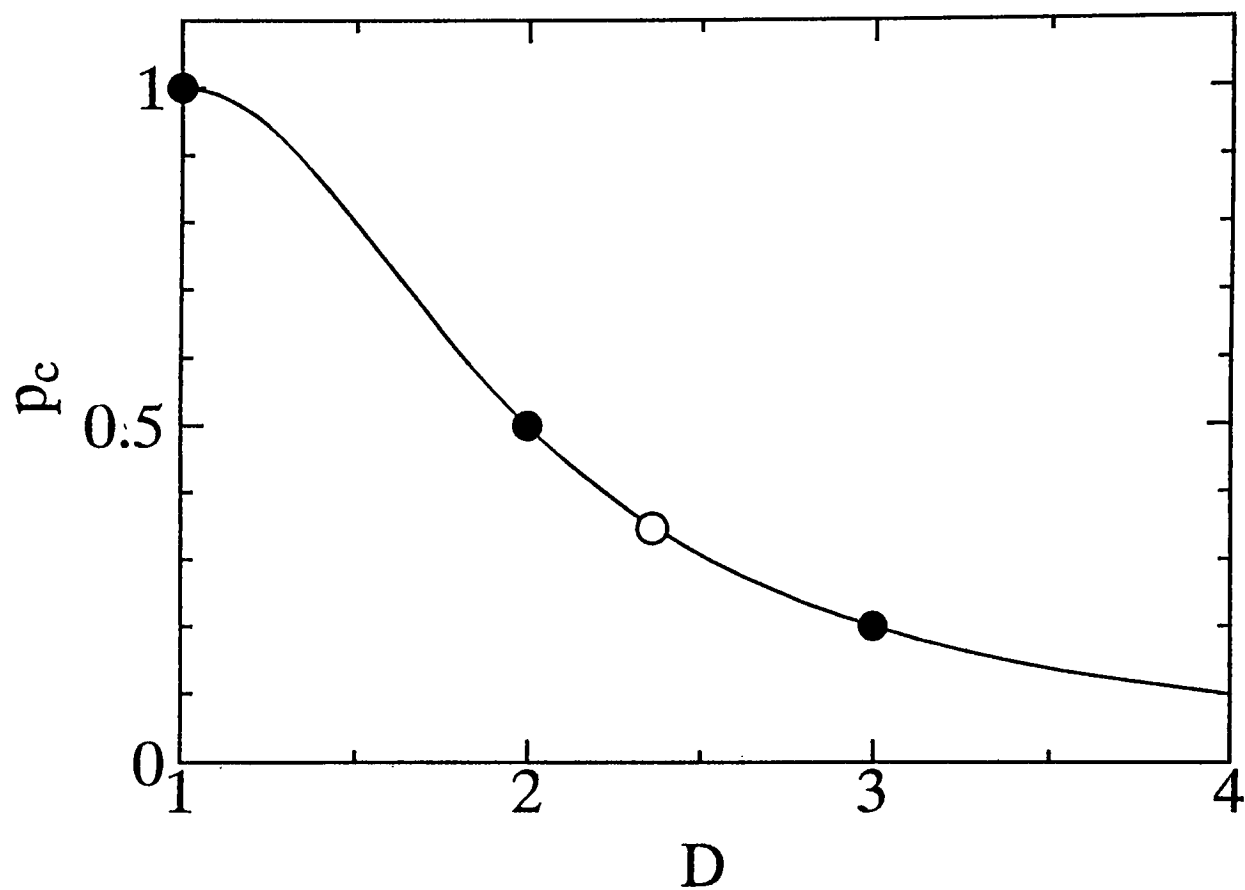


Fig. 23. Dimension dependence of the percolation threshold for close-packed lattice (solid circles). Solid line defines the effective dimension. Open circle corresponds to the BO-C<sub>10</sub>TCNQ LB film.

by

$$\begin{cases} p' &= \frac{p}{f(\sigma)} \\ f(\sigma) &= \frac{a'\{-b+\sqrt{b^2-4a(c-\sigma)}\}}{a\{-b'+\sqrt{b'^2-4a'(c'-\sigma)}\}} \end{cases}, \quad (21)$$

where  $\sigma = \sigma^{2D}(p') = \sigma^{2.4D}(p)$ . In other words, the site occupancy  $p$  is re-scaled by the function  $f(\sigma)$  in order to apply the two-dimensional percolation model. Using the Eq. (15), the values of  $p_1^{th}$  are transformed into  $p_1^{th}$  as listed in Table 6. Thus we study the behavior of the conductance for the 2.4-dimensional percolation path, through the calculation for the two-dimensional percolation path.

The value of  $p_2$  can be roughly estimated from the ratio of X-ray intensity. Considering that the BO-C<sub>10</sub>TCNQ complex itself turns into semiconducting below 130 K and contains water molecules, it is natural to attribute B series to the disordered region. Therefore we consider that both the C series and B series correspond to the disordered CT complex region and only A series corresponds to the metallic region. Then, the values of  $p_2$  is evaluated by

$$p_2^{ob} = \frac{I_{A(1)}}{I_{A(1)} + I_{B(1)} + I_{C(1)}}, \quad (22)$$

which are also listed in Table 6. The values of  $p_2^{ob}$  ( $< 0.3$ ) indicates that more than 70 % of the CT complex are disordered. For the percolation simulation, we adopt the average value  $p_2 = 0.25$ , which is transformed into  $p'_2 = 0.39$  in the modified two-dimensional percolation model.

The temperature dependence of the conductivity is fitted well with  $p'_2 = 0.39$ ,  $C_{ms} = 480$ ,  $E = 120$  K as shown in Fig. 24. In order to obtain a better fit, The values of  $p'_1$  used for the calculation ( $p_1^{cal}$ ) were varied around the theoretical values ( $p_1^{th}$ ) as listed in Table 6. The deviation from  $p_1^{th}$  falls in within 0.03. In spite of the simplicity of the adopted model, the overall behavior of the conductivity, including the gradual metal-nonmetal transition, is well reproduced. The calculated room-temperature conductivity ( $\sigma_{RT}^{cal}$ ) and the temperature with the maximum conductivity ( $T_{max}^{cal}$ ) are also listed in Table 6. The

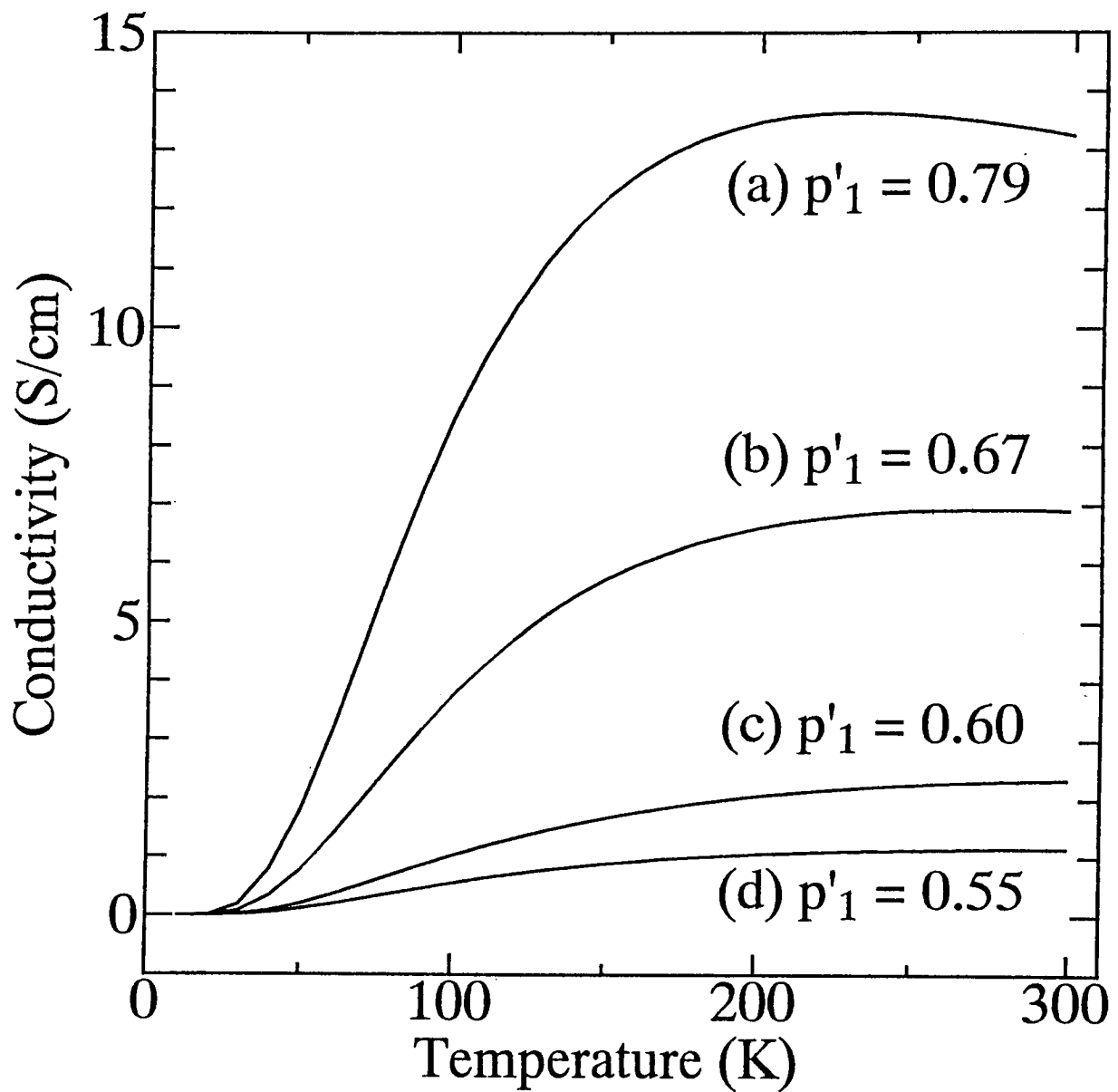


Fig. 24. Simulation results of the electrical conductivity based on the modified two-dimensional MSI percolation model with  $p_2 = 0.39$ ,  $C_{ms} = 480$ ,  $E = 120$  K.

Table 6: Values of parameters related to the simulation based on the modified 2D MSI percolation model

X	1	2	3	4
$\sigma_{RT}^{ob}$ (S/cm)	13.1	7.0	2.6	1.2
$\sigma_{RT}^{cal}$ (S/cm)	13.2	6.9	2.4	1.2
$T_{max}^{ob}$ (K)	230	260	—	—
$T_{max}^{cal}$ (K)	230	280	—	—
$p_1^{th}$	0.71	0.56	0.45	0.38
$p_1^{ih}$	0.78	0.66	0.57	0.52
$p_1^{cal}$	0.79	0.67	0.60	0.55
$p_2^{ob}$	0.28	0.19	—	0.27

quantitative agreement with the experimental results is rather satisfactory. In the boundary model [15,16], the physical interpretation of the variation of  $A$ ,  $\alpha$  and  $E$  is not clear, whereas the physical interpretation of the percolation model is rather straightforward, where the variation depending on the mixing ratio of the constituent molecules is reproduced based on the variation of a parameter describing the ratio ( $p_1$ ).

The room temperature conductivity of the metallic region is calculated to be 55.1 S/cm by setting all sites to be metallic, which is in the same order of the values of some metallic BO complex such as  $BO_m(BF_4)_n$  (60 S/cm) or  $BO_m(NO_3)_n$  (50 S/cm) [36]. Similarly, the room temperature conductivity of the semiconducting region is obtained as 22.2 S/cm, which is also in the same order of the values of some semiconducting BO complex such as  $BO_8(PCA)_4(H_2O)$  (18 S/cm). The value of activation energy used for the fitting is small. This is probably related to the underestimation of the value of  $p_2$ . We estimated the value of  $p_2$  from the ratio of X-ray diffraction intensity, by assuming that the structures of normal CT complex region and the water containing CT complex region are almost the same. However, since the presence of water molecules changes the structure factor of the film, the estimation of the volume ratio of both region is not so simple. Moreover, as the



temperature dependence of the electrical conductivity for the semiconducting region, we assumed the simple exponential form as shown in Eq. (13), however, there is a possibility that the semiconducting region itself possesses a weak metallic properties described by Eq. (3). Although there are above-mentioned problems in the quantitative analysis of the simulation results, the behavior of the electrical conductivity is well understood by the MSI percolation model. The more careful, quantitative analysis should be the future subject.

### 4.3 Effect of domain shape on the dimensionality

In the previous section, we numerically calculated the electrical conductivity of BO-C<sub>10</sub>TCNQ LB films using the modified 2D MSI percolation model, where the parameters are re-scaled according to the effective dimension. The effective dimension of the BO-C<sub>10</sub>TCNQ LB film was estimated to be 2.4 from the experimental percolation threshold. One of the reasons for this deviation from two dimension is ascribed to the effect of the domain shape. According to the AFM topographic images, the domain shape of the CT complex region is needle-like, under which conductive network is formed more easily than in the case of circle-like domains. To take account of the effect of the domain shape, a numerical simulation based on site percolation system has been carried out, assuming that the conductive sites are always selected as linear chains. First, we selected a conductive site randomly in a two-dimensional close-packed triangular lattice, and the direction of the domain extension is also selected randomly. Along this direction,  $L$  successive sites are set to be conductive to form a needle-like domain. Then the next domain is selected in the same way. If we encounter an already conductive site in the course of extending the domain, that site is skipped and the subsequent site is set to be conductive. The percolation threshold ( $p_c$ ) was calculated by simulation using  $30 \times 30$  sites. The calculation was carried out three times and the average values are plotted in Fig. 25, where the percolation threshold decreases with increasing  $L$  as expected.

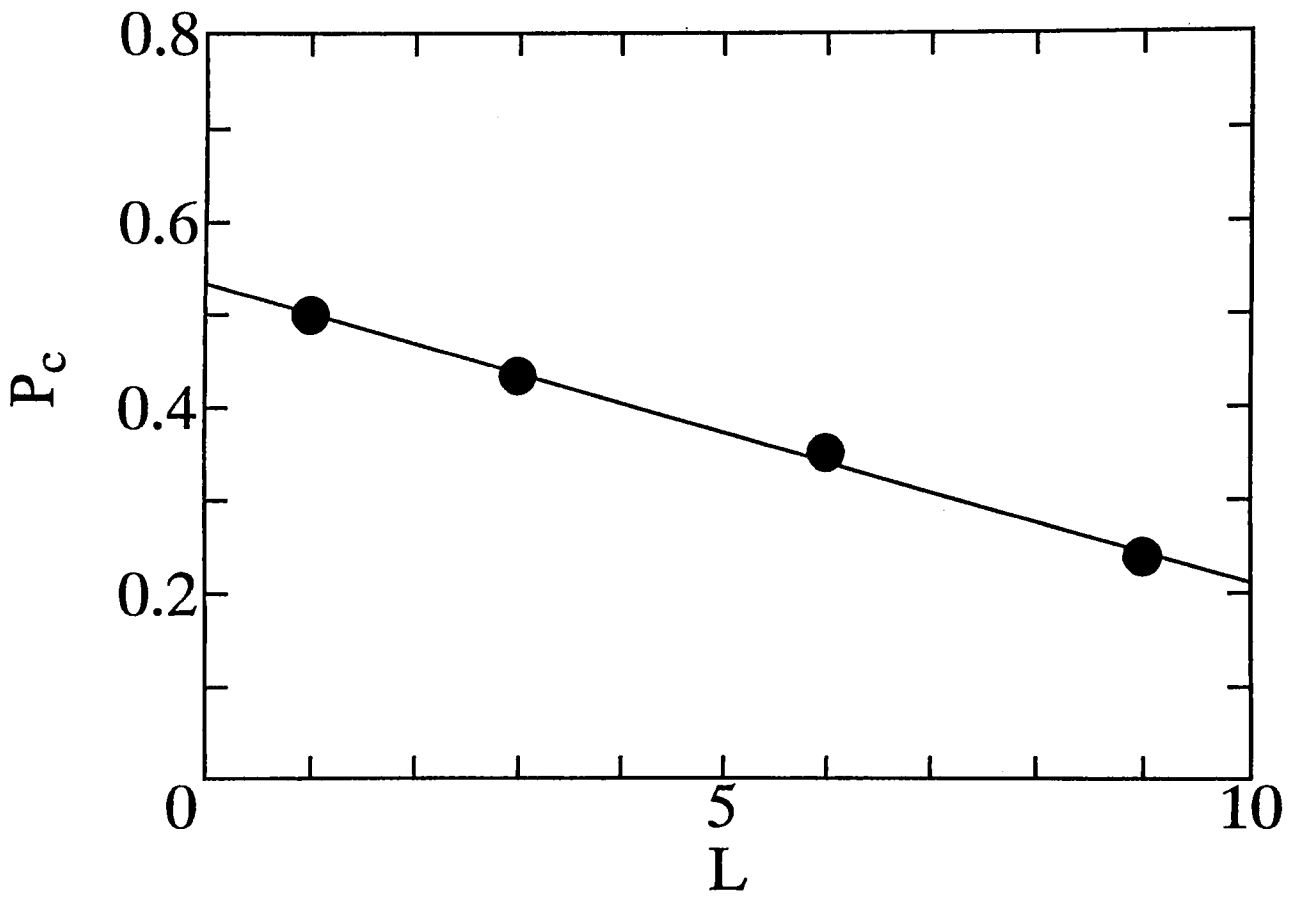


Fig. 25. Relation between the percolation threshold and the length of the domain calculated for the needle-like domains. Solid line is a result of a linear fit.

## 4.4 Effective Medium Theory

In the section 4.2, we numerically calculated the conductance of the MSI percolation model and the variation of temperature dependence of electrical conductivity observed in the BO-C<sub>10</sub>TCNQ LB film was reproduced by varying only one parameter,  $p_1$ . In the present and the following sections, we calculate the conductance of this model in more mathematical manner based on the so-called effective medium theory. First, we explain the theory briefly using a simple example of a binary random resistor network, where the fraction of conductive bond is denoted by  $p$ .

The distribution of potentials in a random resistor network to which a voltage has been applied along one direction may be regarded as due to both an "external field" which increases uniformly, and a fluctuating "local field", whose average over any sufficiently large region becomes zero. The average effects of the random resistors will be represented by an homogeneous effective medium, in which the total field inside is equal to the external field. For simplicity, we consider it to be made up of a set of equal conductances,  $g_e$ , connecting nearest neighboring sites.

In order to determine the value of  $g_e$ , Eq. (12) is rewritten as a matrix equation,

$$\mathbf{W}\mathbf{V} = \mathbf{S}, \quad (23)$$

where  $\mathbf{V}$  is a vector of voltage at each site, expressed in a bra-and-ket notation as

$$\mathbf{V} = \sum_i |i\rangle V_i, \quad (24)$$

while

$$\mathbf{W} = \sum_{ij} |i\rangle (\delta_{ij} \sum_k g_{ik} - g_{ij}) \langle j|, \quad (25)$$

and  $\mathbf{S}$  is zero, except at the two ends of the sample. The potential at each site and the current flow through the medium can be obtained, if we can solve

$$\mathbf{V} = \mathbf{W}^{-1}\mathbf{S}. \quad (26)$$

Thus  $\langle \mathbf{W}^1 \rangle$  contains the information necessary to determine the average conductivity.

To calculate  $\mathbf{W}^{-1}$ , we separate  $\mathbf{W}$  into a homogeneous part,  $\mathbf{W}_e$ , and a fluctuating part,  $\delta\mathbf{W}$  which we may expand whenever  $\mathbf{W}_e$  is not too small:

$$\mathbf{W} = \mathbf{W}_e - \delta\mathbf{W}, \quad (27)$$

where

$$\mathbf{W}_e = \sum_{ij} |i\rangle g_e (z\delta_{ij} - \Delta_{ij}) \langle j|, \quad (28)$$

and  $\Delta_{ij}$  is unity if sites  $i$  and  $j$  are nearest neighbors, while it is zero otherwise.

It is useful to separate  $\delta\mathbf{W}$  into contributions from different bonds  $(i, j)$ ,

$$\delta\mathbf{W} = \sum_{(i,j)} \delta\mathbf{w}_{ij}, \quad (29)$$

where the contribution of the bond  $(i, j)$  is

$$\delta\mathbf{w}_{ij} = (g_e - g_{ij})(|i\rangle\langle i| + |j\rangle\langle j| - |i\rangle\langle j| - |j\rangle\langle i|), \quad (30)$$

which we factorize into

$$\delta\mathbf{w}_{ij} = \delta w_{ij} \mathbf{P}_{ij}, \quad (31)$$

where

$$\delta w_{ij} = 2(g_e - g_{ij}), \quad (32)$$

and  $\mathbf{P}_{ij}$  is a projection operator for the  $ij$ -th bond:

$$\mathbf{P}_{ij} = \frac{1}{2}(|i\rangle - |j\rangle)(\langle i| - \langle j|). \quad (33)$$

These definitions are useful in evaluating the series expansion for  $\mathbf{W}^{-1}$ ,

$$\mathbf{W}^{-1} = \mathbf{W}_e^{-1} \sum_{n=0}^{\infty} [(\sum_{(ij)} \delta w_{ij} \mathbf{P}_{ij}) \mathbf{W}_e^{-1}]^n, \quad (34)$$

since all terms involving repeated powers of a given  $\delta w_{ij}$  can be simplified and collected by introducing a  $t$ -matrix,  $\mathbf{t}_{ij}$ , for the bonds:

$$\mathbf{t}_{ij} = \frac{\mathbf{P}_{ij} \delta w_{ij}}{1 - \delta w_{ij} F_{ij}}, \quad (35)$$

involving only the matrix element of  $\mathbf{W}_e^{-1}$  which is projected by  $\mathbf{P}_{ij}$ :

$$F_{ij} = \frac{1}{2}(\langle i| - \langle j|) \mathbf{W}_e^{-1} (|i\rangle - |j\rangle). \quad (36)$$

The series (34) is expressed in terms of the  $\mathbf{t}_{ij}$ 's as follows,

$$\mathbf{W}^{-1} = \mathbf{W}_e^{-1} + \mathbf{W}_e^{-1} \sum_{(ij)} \mathbf{t}_{ij} \mathbf{W}_e^{-1} + \mathbf{W}_e^{-1} \sum_{(ij)} \mathbf{t}_{ij} \mathbf{W}_e^{-1} \times \sum_{(kl) \neq (ij)} \mathbf{t}_{kl} \mathbf{W}_e^{-1} + \dots \quad (37)$$

From the sum (37), the "best" choice of  $g_e$  is what satisfies

$$\langle \mathbf{t}_{ij} \rangle = 0, \quad (38)$$

since  $\langle \mathbf{W}^{-1} \rangle$  is given by  $\mathbf{W}_e^{-1}$ , with corrections of  $\langle \mathbf{t}_{ij} \mathbf{t}_{kl} \rangle$  or higher order, and  $g_e$  will be a good approximation for the conductance.

By taking the  $\langle i||i\rangle$  matrix element of the equation  $\mathbf{W}_e^{-1} \mathbf{W}_e = 1$ , we obtain

$$Z \langle i|\mathbf{W}_e^{-1}|j\rangle - \sum_k \Delta_{ik} \langle i|\mathbf{W}_e^{-1}|k\rangle = 1. \quad (39)$$

Since  $\langle i|\mathbf{W}_e^{-1}|j\rangle$  is real, we have

$$F_{ij} = \langle i|\mathbf{W}_e^{-1}|i\rangle - \langle i|\mathbf{W}_e^{-1}|j\rangle = 1. \quad (40)$$

Therefore, we have,

$$\mathbf{t}_{ij} = \frac{\mathbf{P}_{ij} z g_e (g_e - g_{ij})}{g_{ij} + (\frac{Z}{2} - 1) g_e}. \quad (41)$$

Thus, the equation  $\langle \mathbf{t}_{ij} \rangle = 0$  is expressed as

$$\int \frac{dg f(g) (g_e - g)}{g + (\frac{Z}{2} - 1) g_e} = 0, \quad (42)$$

using the distribution function of the conductance  $f(g)$ , which is expressed as

$$f(g) = p\delta(g - \alpha) + (1 - p)\delta(g - \beta), \quad (43)$$

in the case of binary random resistor network, where  $\alpha$  and  $\beta$  are the resistances of two kinds of bonds, respectively.

Then Eq.(42) reduces to a quadratic equation for  $g_e$ :

$$(Z - 2)g_e^2 - 2\left\{\left[\frac{Z}{2}p - 1\right]\alpha + \left[\frac{z}{2}(1 - p) - 1\right]\beta\right\}g_e - 2\alpha\beta = 0. \quad (44)$$

The relevant solution of Eq.(44) is

$$g_e = \frac{\frac{1}{z-2}\left\{\left[\frac{z}{2}p - 1\right]\alpha + \left[\frac{z}{2}(1 - p) - 1\right]\beta\right\}}{\sqrt{\left\{\left[\frac{z}{2}p - 1\right]\alpha + \left[\frac{z}{2}(1 - p) - 1\right]\beta\right\}^2 + 2(z - 2)\alpha\beta}}. \quad (45)$$

Now we study the characteristics of this solution. When  $\beta \rightarrow 0$ , Eq. (45) has a simple limiting form:

$$g_e = \alpha\left(\frac{Zp - 2}{Z - 2}\right), \quad (46)$$

and the conductance is reduced according to  $p$ . However, when  $\beta \rightarrow \infty$ , Eq. (45) apparently diversifies, indicating that the theory is essentially an approximation based on the "parallel" connection of two kinds of resistors. This is due to the fact that we averaged  $\langle t_{ij} \rangle$  in respect of conductance. Thus, the theory is valid above the percolation threshold, where the parallel connection is the main contribution, while not valid below the percolation threshold, where the serial connection is the main contribution. However, the MSI percolation model is somewhat complicated, because for the BO-C<sub>10</sub>TCNQ LB film, the amount of the CT complex region is above the percolation threshold, while the amount of the "metallic" CT complex region is below the percolation threshold, indicating that the effective medium theory in this form is not applicable straightforwardly for the MSI percolation model. Below the percolation threshold, it is necessary to modify the theory to be an approximation based on the "serial" connection of the constituent mediums. Such

expression can be obtained by averaging  $\langle t_{ij} \rangle$  in respect of resistance. Then we can calculate the conductance of the BO-C<sub>10</sub>TCNQ LB film in the following two steps. First, we calculate the conductance of the CT complex region by the effective medium theory in respect of resistance. After that, we calculate the conductance of the LB film, by the effective medium theory in respect of conductance.

#### 4.5 Effective Medium Treatment of MSI percolation model

In order to calculate the conductance of the CT complex region, we reconstruct the effective medium theory in terms of resistance. Using

$$\begin{cases} r &= \frac{1}{g} \\ r_e &= \frac{1}{g_e} \end{cases}, \quad (47)$$

Eq. (42) can be written as

$$\int \frac{dr h(r)(r - r_e)}{r_e + (\frac{Z}{2} - 1)r} = 0. \quad (48)$$

For the CT complex region in the BO-C<sub>10</sub>TCNQ LB film, the distribution function of the bond resistance  $h(r)$  is calculated as following. We consider a model of site percolation consisting of metallic sites and semiconducting sites, If the fraction of metallic sites is  $p$ , the probability of finding a bond connecting two metallic sites is yielded by  $p^2$ , while the probability of finding a bond connecting two semiconducting sites becomes  $(1 - p)^2$ . The probability of finding a bond connecting a metallic site and a semiconducting site is given by  $2p(1 - p)$ . Then using the parameters described in the section 4.1,  $h(r)$  is expressed as

$$h(r) = p^2 \delta(r - \frac{T}{C_m}) + 2p(1 - p) \delta(r - [\frac{T}{2C_m} + \frac{1}{2C_s} \exp(\frac{E}{T})]) + (1 - p)^2 \delta(r - \frac{1}{C_s} \exp(\frac{E}{T})), \quad (49)$$

and Eq. (48) becomes a cubic equation

$$r_e^3 + ar_e^2 + br_e + c = 0, \quad (50)$$

where

$$\begin{cases} a &= [\frac{3}{2}(\frac{Z}{2} - 1) - p\frac{Z}{2}]\frac{T}{C_m} + [\frac{3}{2}(\frac{Z}{2} - 1) - (1-p)\frac{Z}{2}]\frac{T}{C_m} \exp(\frac{E}{T}) \\ b &= \frac{1}{2}(\frac{Z}{2} - 1)[(1-p)^2\frac{Z}{2} - 1](\frac{T}{C_m})^2 + (p^2\frac{Z}{2} - 1)(\frac{Z}{2} - 1)[\frac{1}{C_s} \exp(\frac{E}{T})]^2 \\ &\quad + [\frac{Z}{2} + 2Zp(1-p) - 4]\frac{T}{C_m C_s} \exp(\frac{E}{T}) \\ c &= -(\frac{Z}{2} - 1)^2 \frac{T}{C_m} \frac{1}{C_s} \exp(\frac{E}{T}) [\frac{T}{2C_m} + \frac{1}{2C_s} \exp(\frac{E}{T})] \end{cases} \quad (51)$$

Eq. (50) can be expressed in the reduced form,

$$(r_e + \frac{a}{3})^3 + 3\zeta(r_e + \frac{a}{3}) + \eta = 0, \quad (52)$$

where

$$\begin{cases} \zeta &= \frac{1}{3}(3b - a^2) \\ \eta &= \frac{1}{27}(2a^3 - 9bc + 27c) \end{cases} \quad (53)$$

The relevant solution is expressed as

$$r_e = \sqrt[3]{\chi} \cos(\frac{\theta}{3}) - \frac{a}{3}, \quad (54)$$

where

$$\begin{cases} \chi &= \eta^2 + |\eta^2 + 4\zeta^3| \\ \theta &= \tan^{-1}(-\frac{\sqrt{|\eta^2 + 4\zeta^3|}}{\eta}). \end{cases} \quad (55)$$

Accordingly, the conductance of CT complex region is expressed as the function of  $Z, p_2 (= p), C_m, C_s, E$ ,

$$\sigma^{CT}(Z, p_2, C_m, C_s, E) = \frac{1}{r_e}. \quad (56)$$

Prior to apply Eq. (56) to the CT complex region, we consider the dimensionality of the CT complex region. Due to the presence of insulating sites, the number of nearest neighbor sites within the CT complex region is reduced according to the amount of insulating sites. The effective number of nearest neighbor sites is expressed as

$$Z^{eff} = Z^{LB} p_1, \quad (57)$$

where  $Z^{LB}$  is the value in the absence of insulating sites.



Next we apply Eq. (46) to obtain the conductance of the LB film. In Eq. (46),  $p$  represents the fraction of conductive bond. Thus we need to calculate  $p$  from the fraction of conductive sites  $p_1$ . Considering that a bond becomes conductive when both of the connected sites are conductive, the probability of finding conductive bond is given by  $p_1^2$ . In this evaluation, we completely neglected the correlation between bonds: when one bond is conductive, the probability that the successive bond is conductive is given by  $p_1$ . Thus when the number of conductive sites are large,  $p$  approaches to  $p_1$ . On the other hand, when the number of conductive sites are small,  $p$  approaches to  $p_1^2$ . In order to consider the correlation between bonds, we introduce a parameter  $\alpha$  ( $1 \leq \alpha \leq 2$ ), and express the fraction of conductive bond as  $p = p_1^\alpha$  where  $\alpha$  depends on  $p_1$ . Then, the conductance of the LB film is given by

$$\sigma^{LB} = \frac{Zp_1^\alpha - 2}{Z - 2} \sigma^{CT}(Z^{LB} p_1, p_2, C_m, C_s, E). \quad (58)$$

In order to calculate the conductance of the LB film, it is useful to define the relation between the effective number of nearest neighbor sites and the effective demension as,

$$Z^{eff} = D(D + 1). \quad (59)$$

Thus  $D^{LB} = 2.4$  corresponds to  $Z^{LB} = 8.16$ . The electrical conductivity of the LB films was fitted well by eq. (58), with the parameters,  $p_2 = 0.25$ ,  $C_m = 9165$ ,  $C_s = 19.5$ ,  $E = 60$  (K), using  $p_1$  and  $\alpha$  listed in Table 7, as shown in Fig. 25. The values of  $\alpha$  lies between 1 and 2, and  $\alpha$  increases for decreasing  $p_1$ , as expected. The overall characteristics is reproduced and the quantitative agreement is satisfactory. The calculated room-temperature conductivity ( $\sigma_{RT}^{cal}$ ) and the maximum temperature ( $T_{max}^{cal}$ ) are listed in Table 7. From Eq. (58), the physical meaning of variation of temperature dependence is clearly understood in the following way. When  $p_1$  increases,  $Z^{eff}$  increases, that is, the effective dimension of the CT complex region increases with increasing  $p_1$ . When the effective dimension increases,

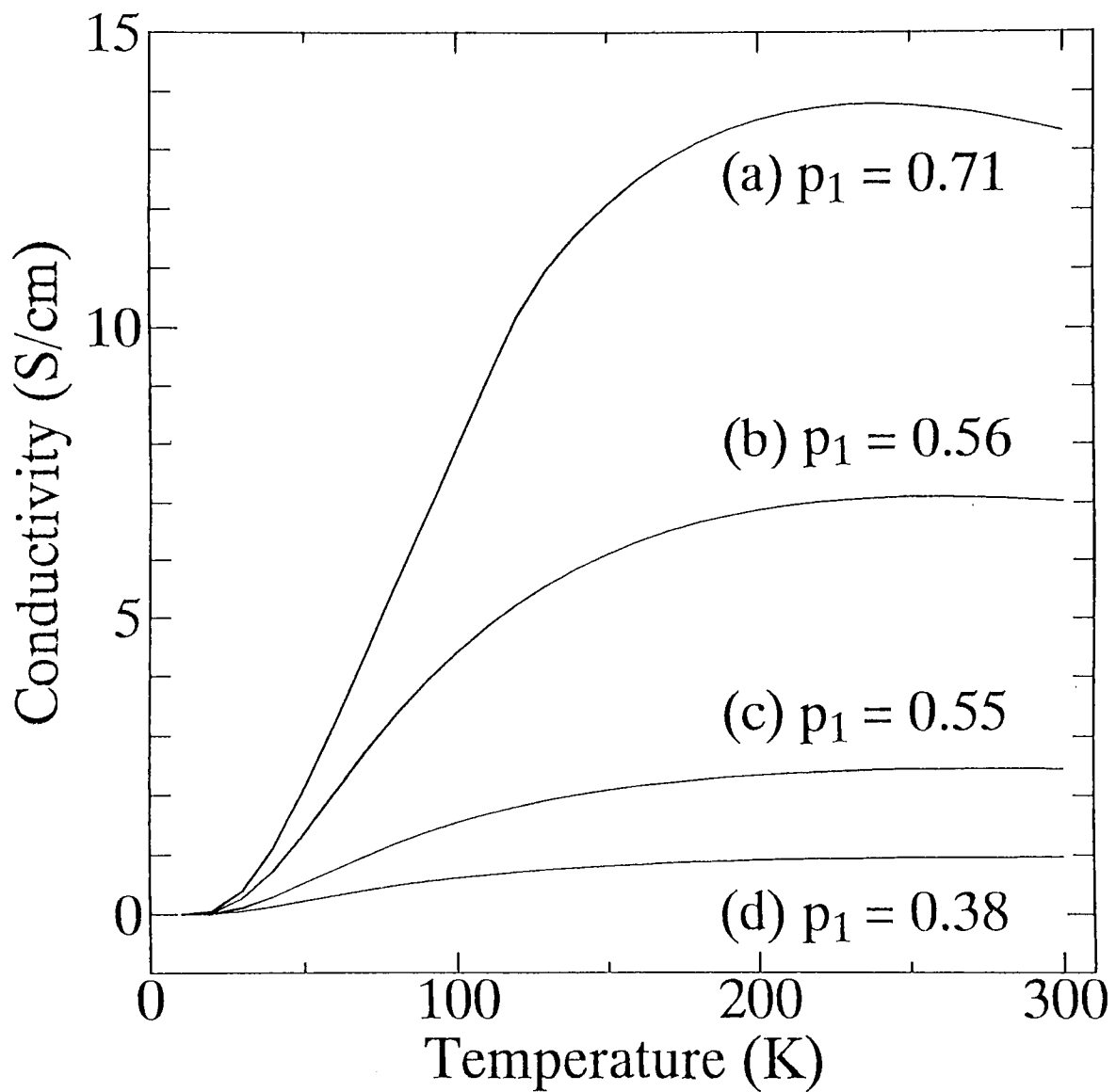


Fig. 26. Temperature dependence of the electrical conductivity calculated by the effective medium treatment of MSI percolation model with  $p_2 = 0.39$ ,  $C_{ms} = 470$ ,  $E = 60$  K.

Table 7: Values of parameters related to the effective medium treatment of the MSI percolation model.

X	1	2	3	4
$\sigma_{RT}^{ob}$ (S/cm)	13.1	7.0	2.6	1.2
$\sigma_{RT}^{cal}$ (S/cm)	13.3	7.0	2.5	1.0
$T_{max}^{ob}$ (K)	240	260	—	—
$T_{max}^{cal}$ (K)	230	280	—	—
$p_1^{th}$	0.71	0.56	0.45	0.38
$\alpha$	1	1.1	1.2	1.2

the number of the parallel conductive path increases and metallic path will be selected more frequently, resulting in the enhancement of metallic properties. The value of the activation energy is smaller than that obtained by the simulation results, probably due to the approximation ignoring the correlation between bonds. The fitting results indicate that the room-temperature conductivity of the metallic region is 30.1 S/cm, which is somewhat smaller than the value obtained by simulation in the section 4.2, but still in the same order of the values of some metallic BO complexes such as  $BO_m(BF_4)_n$  (60 S/cm) or  $BO_m(NO_3)_n$  (50 S/cm) [36]. Similarly, the room temperature conductivity of the semiconducting region is obtained as 16.0 S/cm, which is also somewhat smaller than the value obtained by the simulation, but in the same order of the values of some semiconducting BO complexes such as  $BO_8(PCA)_4(H_2O)$  (18 S/cm). These differences are also ascribed to the approximation ignoring the correlation between bonds.

#### 4.6 Phase diagram of the MSI percolation model

Taking account of the experimental percolation threshold, we can provide a phase diagram of the MSI percolation model in respect of  $p_1$  and  $p_2$  as shown in Fig. 26. The insulating region (I) is yielded by  $p_1 < 0.35$ , while metallic region (M) is given by  $p_1 p_2 > 0.35$ .

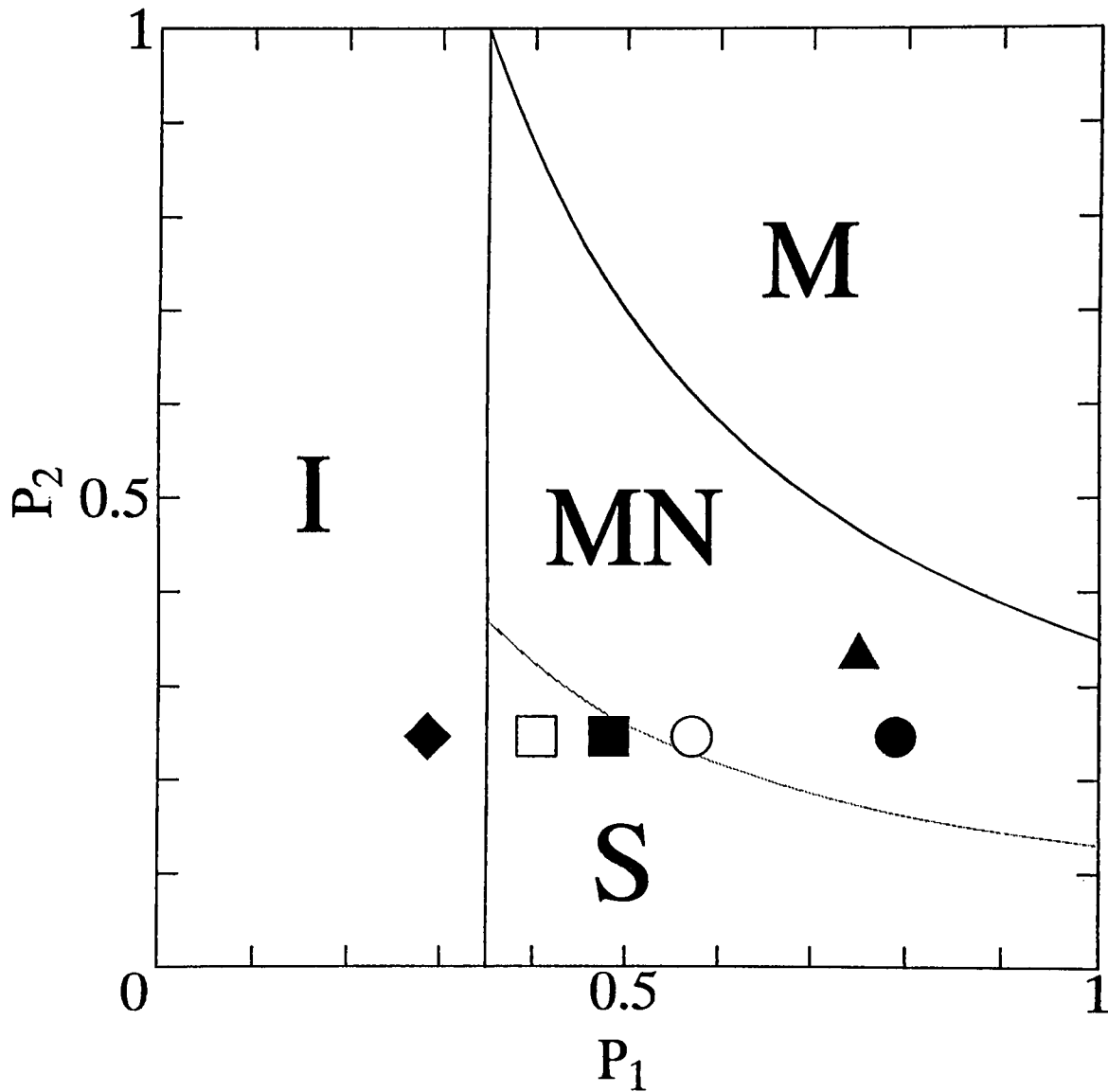


Fig. 27. Phase diagram of the 2.4-dimensional MSI percolation model. M denotes the metallic region, S the semiconducting region, I the insulating region and MN the region in which the gradual metal-nonmetal transition is observed (below 300 K). Solid circle, open circle, solid square, open square and solid rhombus denote the data for BO-C<sub>10</sub>TCNQ LB film with  $X = 1, 2, 3, 4, 6$ , respectively. Solid triangle denotes the data for BO-(MeO)<sub>2</sub>TCNQ LB film.

A gradual metal-nonmetal transition (below 300 K) is observed in the region represented by  $g(p_1) < p_2 < 0.35/p_1$  (MN), where  $g$  is a certain function, which can be determined experimentally. The rest is the semiconducting region (S). When the value of  $E$  is small enough (or the value of  $C_{ms}$  is large enough), the region MN disappears ( $g(p_1) \sim 0.35 / p_1$ ). On the other hand, when the value of  $E$  is large enough (or the value of  $C_{ms}$  is small enough), the region S disappears ( $g(p_1) \sim 0$ ). Considering such opposite extreme expressions, it is natural to assume the form of  $g(p_1)$  as  $g(p_1) = C/p_1$ , where  $C$  is a constant determined by  $E$  and  $C_{ms}$ . In the case of BO-C<sub>10</sub>TCNQ LB film, the value of  $C$  is estimated to be 0.13 from the experimental results shown in Fig. 27.

In order to realize the metallic phase in the phase diagram, it is necessary to increase the value of  $p_2$ . Since  $p_2$  is related to the disorder within the CT complex region, it is required to improve the LB film formation technique so as to suppress the disorder. It is necessary to optimize preparation conditions and constituent molecular species, in order to develop an LB film with metallic conduction in the wider temperature range. The development of BO-(MeO)<sub>2</sub>TCNQ LB film is an example of ways to increase  $p_2$ .

## 5 Characterization of BO-(MeO)<sub>2</sub>TCNQ LB Film

### 5.1 Electrical conductivity

The structure and electronic properties of BO-(MeO)<sub>2</sub>TCNQ LB film have been studied through the measurements of the electrical conductivity, X-ray diffraction and ESR, in a similar way as the BO-C<sub>10</sub>TCNQ LB film.

For the measurements of the electrical conductivity, gold electrodes were evaporated on the hydrophobized surface of the glass substrate before deposition. The temperature dependence of the electrical conductivity was observed down to liquid nitrogen temperature using the four-probe method. Considering the area of one IA molecule (0.2 nm<sup>2</sup>) [34], that of one BO molecule (0.2 nm<sup>2</sup>) [33], and the number ratio of BO to IA (1 : 2), the expected area per molecule of IA within the mixed monolayer on the water surface is 0.6 nm<sup>2</sup>. According to the  $\pi$ -A isotherm shown in Fig. 11, the observed area per molecule of IA at 20 mN/m is 0.3 nm<sup>2</sup>, one half of the expected value. This implies that a bilayer-like structure may be formed on the water surface, although the reason for this is to study. Thus as an average thickness of the bilayers, we tentatively use the value of 4.8 nm, which is twice of the length of IA molecule. Then, the intralayer bulk conductivity at room temperature is evaluated to be 11.3 S/cm. The temperature dependence of the electrical conductivity of the BO-(MeO)<sub>2</sub>TCNQ LB film is shown in Fig. 28. It is noteworthy that the metallic conductance yielding a clear negative temperature-derivative is extended down to 180 K. For comparison, the temperature dependence of the conductivity of the BO-C<sub>10</sub>TCNQ LB film [15] is shown with thin solid line in Fig. 28.

### 5.2 X-ray diffraction

In order to evaluate the structural order in the direction normal to the film plane, X-ray diffraction measurements were carried out using the ordinary  $\theta - 2\theta$  scan method with a

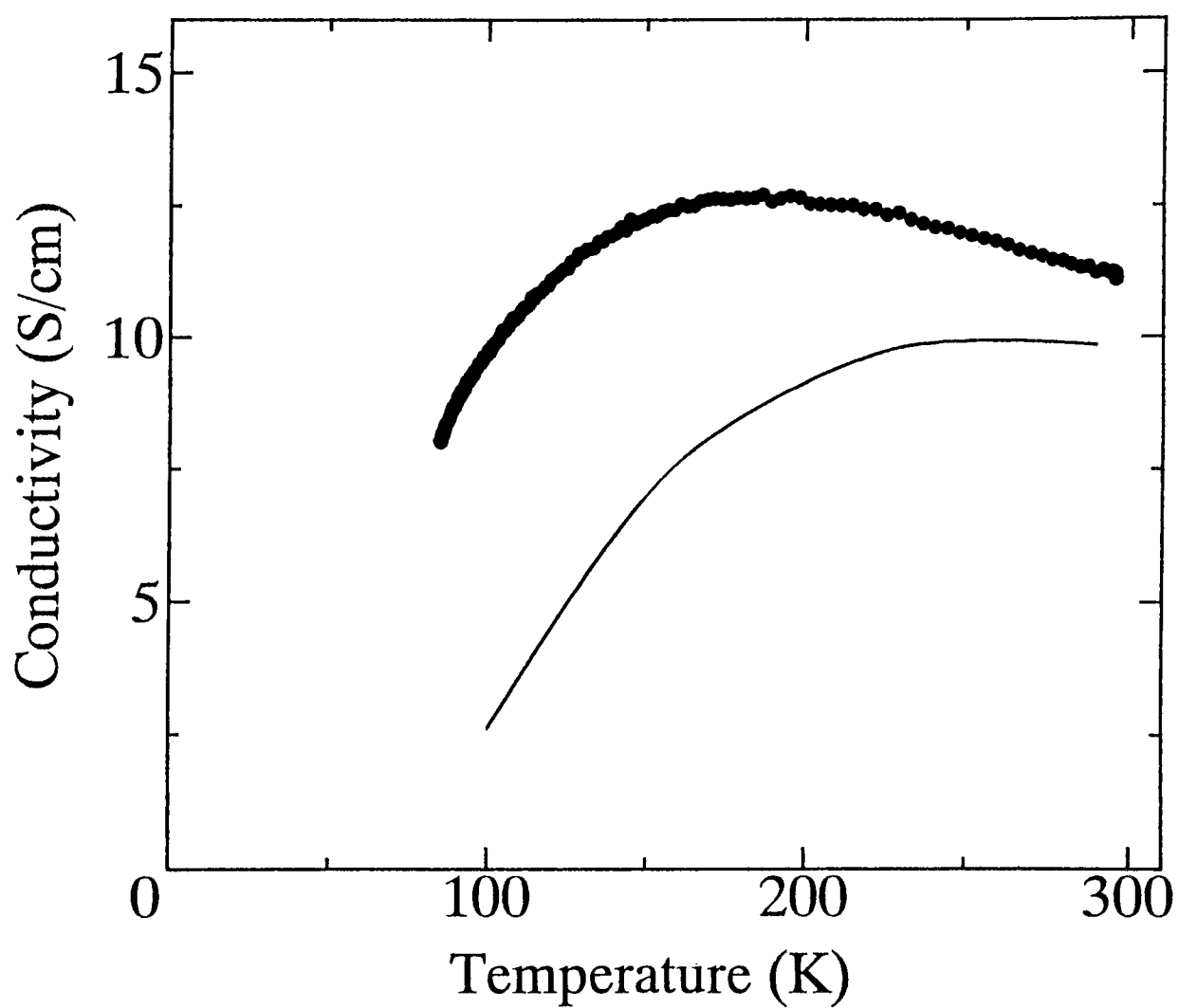


Fig. 28. Temperature dependence of the electrical conductivity for BO-(MeO)<sub>2</sub>TCNQ LB film (closed circles) and that for BO-C<sub>10</sub>TCNQ LB film (solid line).

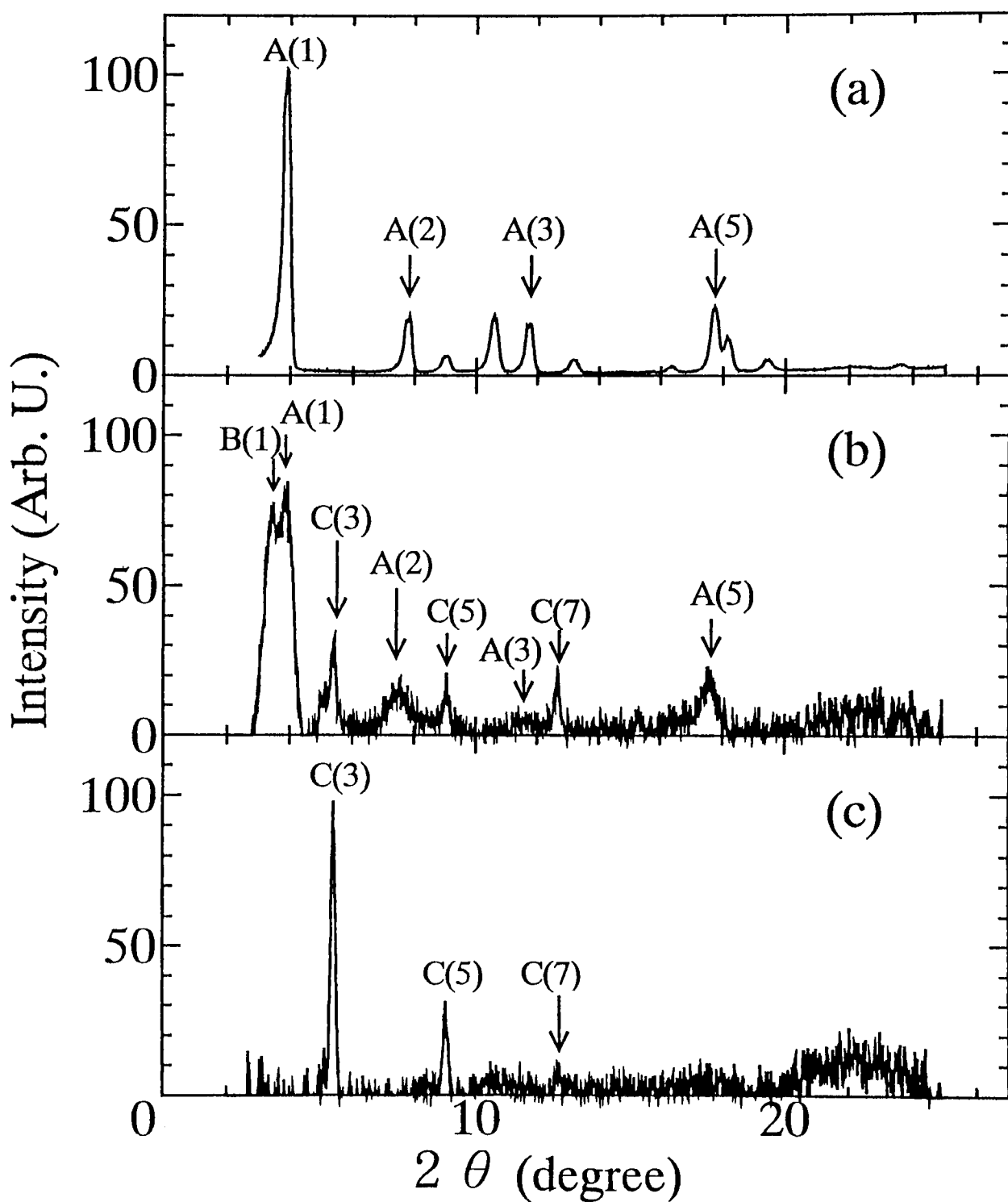


Fig. 29. X-ray diffraction profiles for (a) powder sample of BO-(MeO)<sub>2</sub>TCNQ complex, (b) BO-(MeO)<sub>2</sub>TCNQ LB film and (c) homogeneous LB film of IA .



CuK $\alpha$  source at 40 KV and 200 mA. Due to the lack of heavy atoms and thinness of the film, such a large current was required. For comparison, the X-ray diffraction profile of BO<sub>2</sub>-(MeO)<sub>2</sub>TCNQ CT complex powder sample and the homogeneous LB film of IA are also measured. The observed X-ray diffraction profiles are shown in Fig. 29.

For the BO-(MeO)<sub>2</sub>TCNQ LB film, three diffraction peak series representing different periodicities are discriminated, showing that the film consists of three kinds of domains with different periodicities. The interplanar spacings for the domains are to 2.3 nm (A series), 2.6 nm (B series) and 4.9 nm (C series). Among them, the A series are observed in the profile of BO<sub>2</sub>-(MeO)<sub>2</sub>TCNQ CT complex powder sample, indicating that this structure corresponds to the normal CT complex region. The C series are the same as those observed in the homogeneous LB film of IA, indicating that this domain corresponds to the IA molecule region. On the other hand, the B series are observed only in the BO-(MeO)<sub>2</sub>TCNQ LB film. Taking into account that the A series continuously extends to B series the B series probably corresponds to the CT complex region, which contained water molecules during deposition and possesses a little larger interplanar spacing. Due to the disorder, such regions are expected to possess semiconducting property in the electrical conduction.

### 5.3 Electron spin resonance

In order to characterize the orientation of deposited molecules and the electronic state, ESR measurements were carried out in the X-band (9.4 GHz). The ESR spectra for the BO-(MeO)<sub>2</sub>TCNQ LB film at 10 K with different orientations of the dc magnetic field are shown in Fig. 30. When the dc field is oriented perpendicular to the film plane, two spin species are found, as shown in Fig. 30. They are decomposed by the least-square-fitting method, assuming Lorentzian line shapes, after Ikegami *et al.* [29] When the dc magnetic field is parallel to the film plane, the two spin signals almost overlap, due to nearly equal *g*-values. This anisotropy strongly indicates that the CT complex molecules are highly

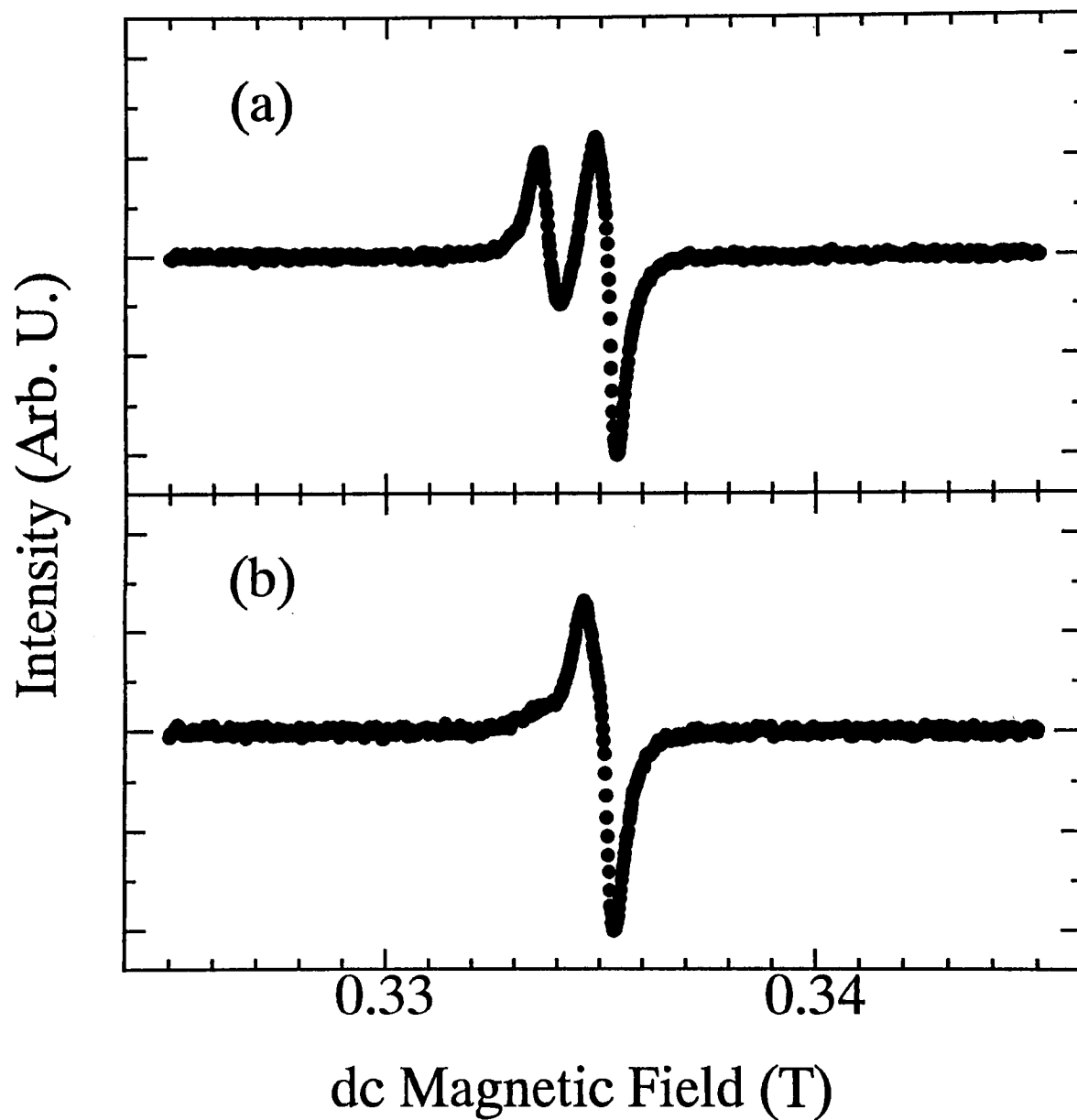


Fig. 30. ESR spectra at the X-band at 10 K for BO-(MeO)<sub>2</sub>TCNQ LB film with dc magnetic fields (a) perpendicular and (b) parallel to the film plane.

oriented within the film. The spin species with larger  $g$ -value (hereafter referred to as species I) and that with smaller  $g$ -value (species II) are ascribed to BO and  $(\text{MeO})_2\text{TCNQ}$ , respectively, in analogy to the BO- $\text{C}_{10}\text{TCNQ}$  LB film [29]. From the similarity of the  $g$ -value anisotropy of species I we find that the long axis of BO is almost perpendicular to the film plane [30].

The  $g$ -value, spin susceptibility ( $\chi_S$ ) and line width ( $\Gamma$ ) under a configuration with the dc magnetic field perpendicular to the film plane yielded by the fitting are shown as functions of temperature in Fig. 31. Above 200 K, the spectra have been fitted by a single Lorentzian, since the intensity of the species II is too small to discriminate. We find that species I shows an almost temperature-independent, Pauli-like  $\chi_S$  above 50 K, indicating the presence of metallic domains within the film. The slight decrease of  $\chi_S$  with decreasing temperature is reminiscent of the enhanced Pauli susceptibility due to the electron correlation like the case of TTF-TCNQ [37]. Such behavior is commonly observed in some BO complexes [38]. The rapid decrease of  $\chi_S$  below 50 K accompanied by the sudden decrease of  $\Gamma$  is likely imply that the metallic domain undergoes a metal-insulator transition as found in  $(\text{BEDT-TTF})_3(\text{ReO}_4)_2$  [39]. The increase of  $\chi_S$  below 20 K implies the presence of a localized part resulting in a Curie-like  $\chi_S$ , but this can be attributed to a coexisting localized part due to disorders. For species II, the spin susceptibility exhibits typical Curie-like temperature dependence, indicating that it is due to localized spins in  $(\text{MeO})_2\text{TCNQ}$ . The line width for species I decreases with decreasing temperature as shown in Fig. 31. Taking into account the large  $g$ -value, indicating rather large spin-orbit interaction, the behavior is ascribable to the Elliott mechanism [31], which is typical for conduction electrons and supports the presence of metallic phases, even if they are compartmentalized by the IA molecules and disordered regions.

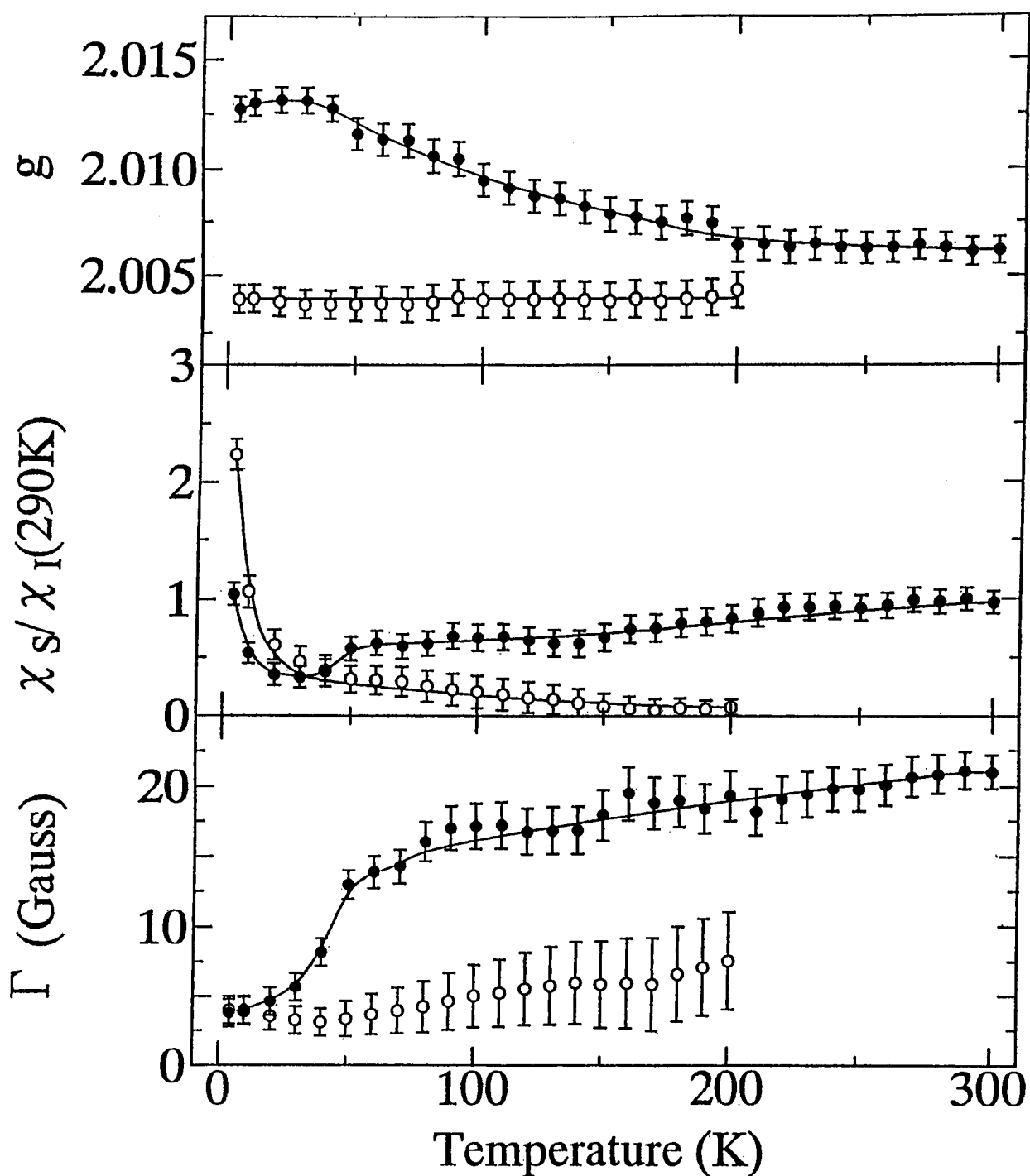


Fig. 31.  $g$ -value, spin susceptibility ( $\chi_s$ ) and line width ( $\Gamma$ ) of BO-(MeO)<sub>2</sub>TCNQ LB film derived from fitting results of the ESR spectra.  $\chi_s$  is normalized by the room-temperature value for species I ( $\chi_I(290\text{ K})$ ). Closed circles denote the data for the species I and open circles for species II. Solid lines are guides for the eye. Errors are due to the uncertainty in decomposition.

## 5.4 Analysis based on the MSI percolation model

Since the results of X-ray and ESR measurements indicate the coexistence of metallic region and semiconducting region, the temperature dependence of electrical conductivity for the BO-(MeO)<sub>2</sub>TCNQ LB film can also be described by the MSI percolation model. For the values of  $E$ ,  $C_{ms}$  and effective dimension, we tentatively adopted those for the BO-C<sub>10</sub>TCNQ LB film. Considering that the ratio of BO to (MeO)<sub>2</sub>TCNQ is 2 : 1, the value of  $p_1$  was estimated to be 0.67, which is transformed into 0.75 by Eq. (21). Then we fitted the temperature dependence of the BO-(MeO)<sub>2</sub>TCNQ LB film with the modified 2D MSI percolation model. The experimental data were fitted with  $p_2 = 0.33$  as shown in Fig. 32. According to the phase diagram in Fig. 27, the development of this film corresponds to the increase of  $p_2$ , as shown by the solid triangle. The physical meaning of the increase of  $p_2$  is the decrease of disorder within the CT complex region, resulting in the improvement of metallic properties. We accomplished this by molecular design approach based on the molecular orbital calculation and by making use of the self-assembling ability of BO molecules.

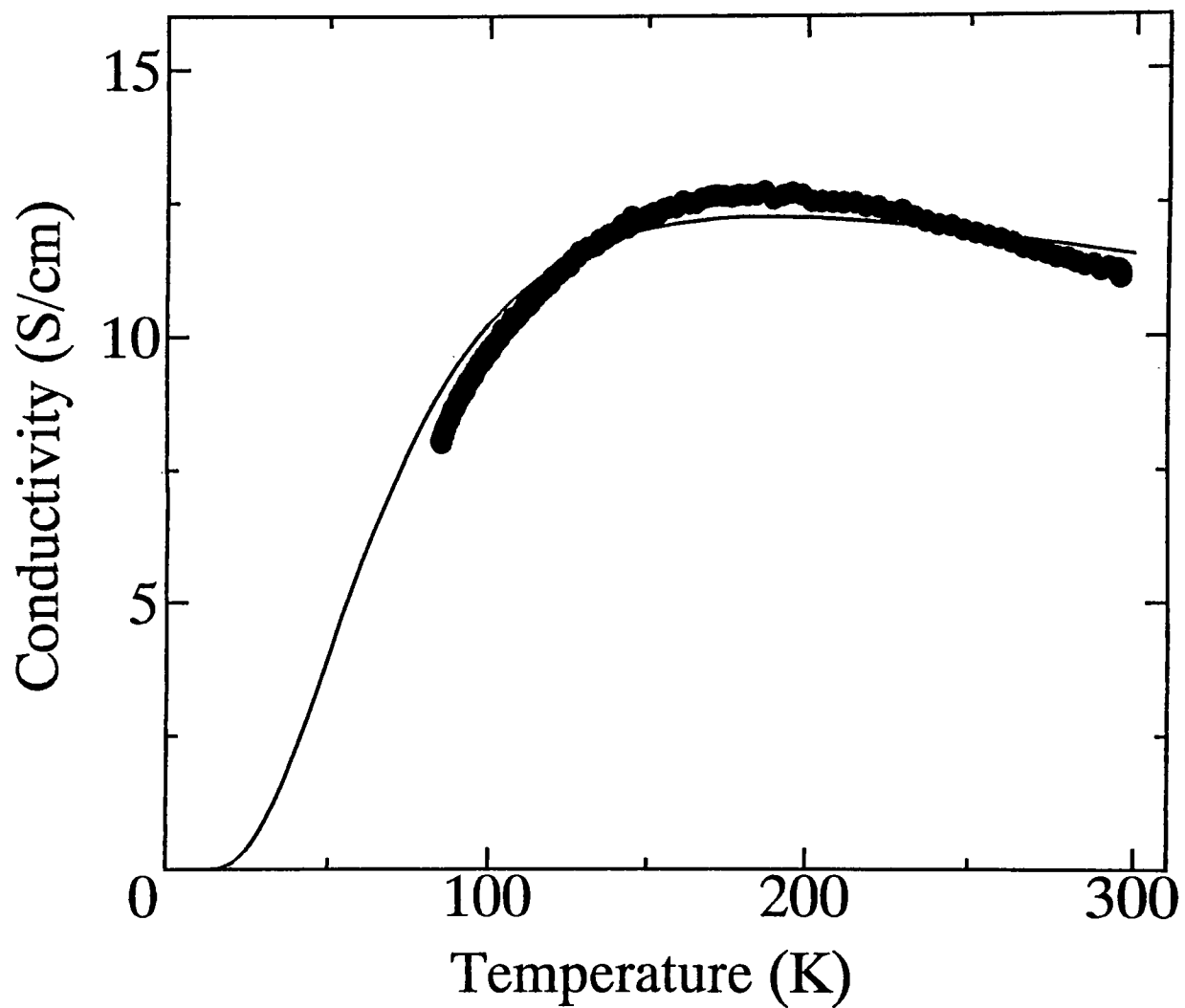


Fig. 32. Calculated electrical conductivity based on the modified 2D MSI percolation model (solid line) and the experimental data for the BO-(MeO)<sub>2</sub>TCNQ LB film (solid circles).

## 6 Conclusion

In order to study the structure and electronic properties of the LB film consisting of BO-C<sub>10</sub>TCNQ and IA, which is known to exhibit a metallic conduction around room temperature, the electrical conductivity, X-ray diffraction, ESR and AFM measurements have been carried out for samples with different ratio of the CT complex to IA.

The temperature dependence of the electrical conductivity varies drastically according to the ratio and the metallic property is suppressed for larger amount of IA. The results of X-ray diffraction indicate that the LB film is compartmentalized into the domain structure. In addition to the normal CT complex region and the IA region, we find a disordered CT complex region with enlarged lattice spacings within the BO-C<sub>10</sub>TCNQ LB film, presumably due to the involvement of water molecules. The anisotropy of ESR spectra indicates that the CT complex molecules are highly oriented within the stacking direction. The  $g$ -values, spin-susceptibility ( $\chi_s$ ) and line width ( $\Gamma$ ) are yielded by fitting of the spectra. Although the apparent nonmetallic behavior is observed below 230 K in the macroscopic electrical conductivity, the results of the spin susceptibility and the ESR line width imply the presence of metallic region down to 50 K. The semiconducting electrical conductivity below 230 K is ascribable to the disordered CT complex region. The AFM imaging of the BO-C<sub>10</sub>TCNQ LB film indicates that the domain shape of the CT complex region is needle-like rather than circle-like.

Taking into account that the film is an inhomogeneous system, the electrical conductance should be understood in terms of the mesoscopic structure of the film. Thus we considered a two-dimensional percolation system consisting of three kinds of sites, such as metallic, semiconducting and insulating sites (MSI percolation model). The temperature dependence of the electrical conductivity has been explained by this model with some modification. Since the effective dimension of the BO-C<sub>10</sub>TCNQ LB film is estimated to be 2.4 from

the percolation threshold, the parameters are re-scaled so as to apply the simulation in two-dimension. The deviation of the effective dimension from two is due to the unevenness of the LB layer and the effect of the domain shape. Thus the variation of the temperature dependence of the electrical conductivity as a function of the mixing ratio of the constituent molecules has been reproduced well. The semiconducting behavior with small activation energy  $E \simeq 120$  K is ascribable to the effect of disorders induced by absorbed water molecules in the CT complex region.

In addition to the simulation, the approximate expression of the conductivity for the MSI percolation model was calculated using the effective medium theory. The characteristic behavior of the electrical conductivity is interpreted in terms of effective dimension of the CT complex region. Based on the MSI percolation model, we derived a phase diagram describing the conducting properties and discussed the methods to realize better conductors.

In order to improve the metallic properties of the BO-C<sub>10</sub>TCNQ LB film, it is necessary to diminish disorders in the CT complex region. For this purpose, we studied the properties of BO and TCNQ molecules through the Hückel MO calculation. Based on the charge-distribution yielded by the HOMO or LUMO, it is concluded that BO is hydrophobic while TCNQ is hydrophilic. In addition, due to a self-assembling ability of BO, the charge-transfer molecular pairs form an amphiphilic sheet with a pair of hydrophilic and hydrophobic surfaces. In other words, a pair of BO and TCNQ molecules is expected to possess a potential to create an amphiphilic CT complex by itself. With this point of view, we have searched for another TCNQ derivative which forms a metallic CT complex with BO. As a result, a stable, highly conductive Langmuir-Blodgett film was developed using a CT complex of BO and dimethoxytetracyanoquinodimethane ((MeO)<sub>2</sub>TCNQ). The metallic properties of this film is considerably improved compared to those of BO-C<sub>10</sub>TCNQ LB film.



The room-temperature conductivity is larger and a clear negative temperature-derivative of the conductivity was extended down to 180 K. The results of X-ray diffraction measurements also indicates the presence of disordered CT complex region due to contained water molecules as in the case of BO-C<sub>10</sub>TCNQ LB films. The anisotropy of the ESR spectra indicates that the CT complex molecules are highly oriented in the stacking direction. The  $g$ -values, the paramagnetic spin susceptibility ( $\chi_s$ ) and ESR line width ( $\Gamma$ ) are obtained by the fitting of the ESR spectra. A relatively large  $g$ -value, almost temperature-independent  $\chi_s$  and decreasing  $\Gamma$  with decreasing temperature indicate that the metallic phase is retained down to 50 K.

## Acknowledgment

The studies presented in this thesis have been carried out at Department of Physics, Faculty of Science, Kyoto University. The author is grateful to Professor T. Ishiguro for his valuable discussions and instructions. He would like to thank Professor G. Saito, Professor H. Yamochi and S. Horiuchi for providing the BO-based CT complexes and for their valuable discussions. He would like to express his gratitude to Professor Y. Nogami for performing the X-ray diffraction measurements. He is also indebted to Dr. Kan-no, M. Shirai for their kind help on ESR measurements.

The author is also grateful to his parents and his parents-in-law for their encouragement and financial support. Finally, he would like to express his heartfelt gratitude to his beloved wife, Tomomi, for her constant encouragement and mental support throughout the period of this work.

## References

- [1] Nakamura T., Tachibana H., Matsumoto M., Tanaka M. and Kawabata Y., *Lower-Dimensional Systems and Molecular electronics* (Edited by Metzger R. M. *et. al.*), p. 519. Plenum Press, New York (1991).
- [2] Matsumoto M., Tachibana H. and Nakamura T., *Organic Conductors* (Edited by Farges J. P.), p. 759. Narcel Dekker, Inc., New York (1994).
- [3] Kagoshima S., Sambongi T. and Matsunaga Y., *One-dimensional Conductors*, Shokabo, Tokyo (1987) [in Japanese].
- [4] Ishiguro T. and Yamaji K., *Organic Superconductors*, Springer-Verlag Press, Berlin (1990).
- [5] Barraud A., Lesieur P., Ruaudel-Teixier A., and Vandevyver M., *Thin Solid Films* **134**, 195 (1985).
- [6] Nogami Y., Hamanaka H. and Ishiguro T., *J. Phys. Soc. Jpn.* **60**, 1860 (1991).
- [7] Nogami Y., Ogasawara K., Takeuchi S., Ishiguro T., Ohsumi K. and Shimizugawa Y., *Mat. Res. Soc. Symp. Proc.* **247**, 835 (1992).
- [8] Nogami Y., Ogasawara K., Takeuchi S., Ishiguro T., Nakajima T., Ohsumi K. and Shimizugawa Y., *J. Phys. Soc. Jpn.* **62**, 3114 (1993).
- [9] Ogasawara K., Nogami Y. and Ishiguro T., *J. Phys. Soc. Jpn.* **63**, 1994 (1994).
- [10] Ikegami K., Kuroda S., Saito M., Saito K., Sugi M., Nakamura T., Matsumoto M. and Kawabata Y., *Phys. Rev.* **B35**, 3667 (1987).
- [11] Nakamura T., Matsumoto M., Tachibana H., Tanaka M., Manda E. and Kawabata Y., *Thin Solid Films* **178**, 413 (1989).
- [12] Ikegami K., Kuroda S., Sugi M., Nakamura T., Tachibana H., Matsumoto M. and Kawabata Y., *J. Phys. Soc. Jpn.* **61**, 3752 (1992).
- [13] Miura Y. F., Takenaga M., Kasai A., Nakamura T., Matsumoto M. and Kawabata Y., *Jpn. J. Appl. Phys.* **30**, 3503 (1991).

- [14] Matsuzaki H., Ogasawara K., Ishiguro T., Nogami Y., Taoda M., Tachibana H., Matsumoto M. and Nakamura T., *Synth. Met.* **74**, 251 (1995).
- [15] Nakamura T., Yunome G., Azumi R., Yumura M., Matsumoto M., Horiuchi S., Yamochi H. and Saito G., *Synth. Met.* **55**, 3853 (1994).
- [16] Nakamura T., Yunome G., Azumi R., Tanaka M., Tachibana H., Matsumoto M., Horiuchi S., Yamochi H. and Saito G., *J. Phys. Chem.* **98**, 1882 (1994).
- [17] Takenaga M., Abdulla A., Kasai A., Nakamura A., Nakamura T., Matsumoto M., Horiuchi S., Yamochi H. and Saito G., *Appl. Phys. Lett.* **64**, 2602 (1994).
- [18] Epstein A. J., Conwell E. M., Sandman D. J., Miller J. S., *Solid State Commun.* **23**, 355 (1977).
- [19] Epstein A. J., Conwell E. M., *Solid State Commun.* **24**, 627 (1977).
- [20] Van-Catledge F. A., *J. Org. Chem.* **45**, 4801 (1980).
- [21] Pockels A., *Nature* **43**, 437 (1891).
- [22] Pockels A., *Nature* **46**, 418 (1892).
- [23] Pockels A., *Nature* **48**, 152 (1893).
- [24] Lord Rayleigh, *Philos. Mag.* **48**, 321 (1899).
- [25] Blodgett K. B., *J. Am. Chem. Soc.* **57**, 1007 (1935).
- [26] Blodgett K. B. and Langmuir I., *Phys. Rev.* **51**, 964 (1937).
- [27] Yamochi H., Horiuchi S., Saito G., Kusunoki M., Sakaguchi K., Kikuchi T. and Sato S., *Synth. Met.* **56** (1994) 2096.
- [28] Ogasawara K., Ishiguro T., Horiuchi S., Yamochi H. and Saito G., *Jpn. J. Appl. Phys.* **35**, L571 (1996).
- [29] Ikegami K., Kuroda S., Nakamura T., Yunome G., Matsumoto M., Horiuchi S., Yamochi H. and Saito G., *Phys. Rev.* **B49**, 10806 (1994).

- [30] Ikegami K., Kuroda S., Nakamura T., Azumi R., Yunome G., Matsumoto M., Horiuchi S., Yamochi H. and Saito G., *Synth. Met.* **71**, 1909 (1995).
- [31] Elliott R. J., *Phys. Rev.* **96**, 266 (1954).
- [32] Kirkpatrick S., *Rev. Mod. Phys.* **45**, 574 (1973).
- [33] Shibaeva R. P and Zavodnik V E., *Crystallogr. Rep.* **38**, 195 (1993).
- [34] Meyer E., Howald L., Overney P. M., Heinzelmann H., Frommer J., Güntherodt H. J., Wagner T., Schier H. and Roth S., *Nature* **349** (1991) 398.
- [35] Ziman J. M., *Models of Disorder*, p. 375. Cambridge University Press, Cambridge (1979).
- [36] Wudl F., Yamochi H., Suzuki T., Isotalo H., Fite C., Liou K., Kasmai H. and Srdanov G., *The Physics and Chemistry of Organic Superconductors, Springer Proceedings in Physics, Vol 51* (Edited by Saito G. and Kagoshima S.), p. 358. Springer-Verlag Press, Berlin (1990).
- [37] Y Tomkiewicz, A. R. Taranko and J. B. Torrance: *Phys. Rev.* **B15** (1977) 1017.
- [38] Beno M. A., Wang H. H., Carlson K. D., Kini A. M., Frankenbach G. M., Ferraro J. R., Larson N., McCabe G. D., Thompson J., Purnama C., Vashon M., Williams J. M., Jung D. and Whangbo M. -H., *Mol. Cryst. Liq. Cryst.* **181** (1990) 145.
- [39] Carneiro K., Scott J. C. and Engler E. M., *Solid State Commun.* **50** (1984) 477.